International Journal of Earth Sciences (2022) 111:379–399
https://doi.org/10.1007/s00531-021-02119-4

ORIGINAL PAPER

Giant (30 km-diameter) silicic caldera of K/Pg boundary age in the northwestern Deccan Traps: the Alech Hills, Saurashtra

Hetu Sheth[1] · Anmol Naik[1] · Janisar M. Sheikh[2] · Alok Kumar[2]

Received: 7 July 2021 / Accepted: 20 September 2021 / Published online: 2 November 2021

Abstract

Voluminous silicic (rhyolitic–dacitic) eruptive units overlie mafic lavas in many continental flood basalt (CFB) provinces of the world. These silicic units comprise lavas as well as pyroclastic deposits, including lava-like ignimbrites, and many were erupted from identified calderas. Silicic volcanic units are widespread in the northern and northwestern parts of the Deccan Traps CFB province of India, particularly the Saurashtra peninsula. In the Alech Hills in Saurashtra, whose geology is poorly known, basal mafic lavas are intruded by a ring dyke of granophyre with a diameter of 30 km. Inside this ring, silicic eruptive units are exposed. The lowest and most extensive unit is a grey, feldspar-phyric, ≥ 3.8 km^3 flood rhyolite lava. This is overlain successively by rheomorphic and lava-like ignimbrites, eutaxitic ignimbrites, and non-welded tuffs and breccias. Based on a combination of geological features, such as the large granophyre ring dyke, the effusive and explosive rhyolite volcanism, fault-controlled arcuate and annular ridges of the rhyolites, possible caldera-collapse mesobreccias, and widespread hydrothermal alteration, we recognize the Alech Hills as a giant (30 km-diameter, 660 km^2) effusive-explosive silicic caldera. A recently published CA-ID-TIMS $^{206}Pb/^{238}U$ date of 65.765 ± 0.018 Ma (2σ) for the granophyre ring dyke suggests that the Alech Hills caldera formed contemporaneously with the K/Pg boundary mass extinction, and may have significantly contributed to it.

Keywords Rhyolite · Ignimbrite · Caldera · Flood basalt · Deccan Traps · K/Pg boundary

Introduction

Continental flood basalt (CFB) volcanism represents intense igneous activity in which millions of cubic kilometers of mantle-derived mafic magma are transported to the Earth's surface to erupt as lavas, within relatively short time periods (e.g., Sheth 2018 and references therein). CFB volcanism commonly also includes silicic (rhyolite–dacite) volcanism, typically during its late stages (e.g., Halder et al. 2021). The silicic eruptive units, often of significant volume, are erupted both effusively (forming lava flows and domes) and explosively (forming pyroclastic deposits such as ignimbrites) (e.g., Ayalew et al. 2002; Sheikh et al. 2020a,b). Explosive eruptions can inject ash and magmatic gases to much greater heights in the atmosphere than effusive eruptions, with correspondingly significantly wider distribution (e.g., Self 2006; Cassidy et al. 2018). Therefore, silicic volcanism in CFB provinces is an important topic of study with implications for the likely environmental impact of the flood volcanism. This is especially so when the CFB volcanism is known to have overlapped with a major mass extinction, such as the ~ 65.5 Ma Deccan Traps of India (Fig. 1a) and the Cretaceous/Palaeogene (K/Pg) boundary mass extinction (e.g., Baksi 2014).

The Deccan Traps are dominated by tholeiitic (subalkalic basalt and basaltic andesite) lavas which cover 500,000 km^2 of west-central India and reach a thickness of > 2 km in the Western Ghats escarpment (Krishnamurthy 2020; Kale et al. 2020; Fig. 1a). Post-flood basalt silicic lavas and ignimbrites are widespread in the northern and northwestern parts of the Deccan Traps, particularly the Saurashtra peninsula (Fig. 1b) (Fedden 1884; Subba Rao 1971; Krishnamacharlu 1974; Misra 1999), and this silicic volcanism has notable similarities to that of the Snake River Plain in the western USA (Sheikh et al. 2020a,b; Naik

✉ Hetu Sheth
hcsheth@iitb.ac.in

[1] Department of Earth Sciences, Indian Institute of Technology Bombay, Powai, Mumbai 400076, India

[2] Centre of Advanced Study in Geology, Institute of Science, Banaras Hindu University (BHU), Varanasi 221005, India

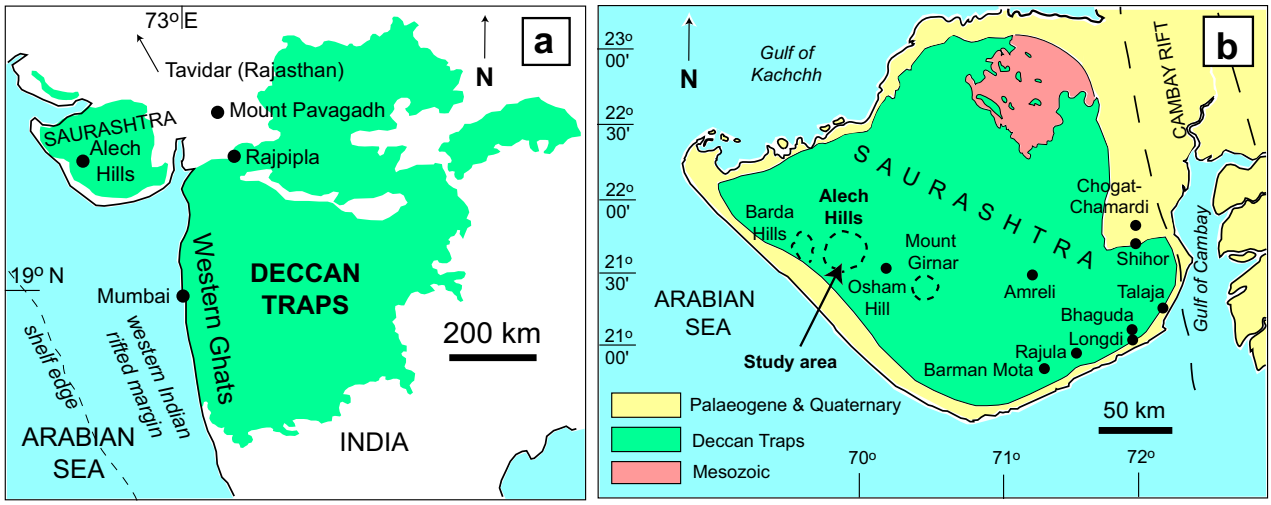

Fig. 1 **a** Geological map of the Deccan Traps CFB province (light green) showing the location of Alech Hills, the study area. **b** Geological map of the Saurashtra peninsula, modified from Cucciniello et al. (2019). Filled circles in (**a**, **b**) denote other localities with notable rhyolites and dacites, with the following coordinates: Barman Mota, N 20° 58′ 58.30″, E 71° 19′ 28.08″; Rajula, N 21° 01′ 57.68″, E 71° 26′ 13.72″; Osham Hill, N 21° 38′ 17.60″, E 70° 16′ 32.20; Bhaguda, N 21° 15′ 08.60″, E 71° 53′ 43.41″; Mount Pavagadh, N 22° 27′ 49.20′, E 73° 30′ 55.30″

et al. 2021). However, the locations and nature of eruptive vents of the northern–northwestern Deccan silicic units are largely unknown, partly because of considerable erosion and limited field studies. Specifically, no silicic calderas corresponding to those known in the Snake River Plain-Yellowstone volcanic province (Ellis et al. 2013; Knott et al. 2016), the Scottish Hebridean CFB province (Emeleus and Bell 2001), or the Etendeka CFB province (Korn and Martin 1954; Milner et al. 1992), for example, are recognised in the northern–northwestern Deccan Traps.

Calderas are important for understanding magma transport into, storage and differentiation within, and eruption from, shallow-level reservoirs, aided by tectonic movements (e.g., Gudmundsson 2015, 2020). Explosive eruptions, particularly from "giant" calderas several tens of kilometers in diameter (Francis 1983), are catastrophic events that significantly affect the atmosphere and the biosphere (Branney and Acocella 2015). Should silicic calderas be found to exist in the Deccan Traps—as they do in other CFB provinces—this would significantly improve our understanding of the physical geological development of Deccan CFB volcanism and its potential contribution to the K/Pg boundary environmental changes. Here, we present data on the geology and eruptive stratigraphy, outcrop structures, and textures of rhyolitic rocks of the Alech Hills in Saurashtra, in the northwestern Deccan Traps (Fig. 1b). These data lead us to recognize the Alech Hills as a giant (30 km-diameter) silicic caldera.

Geology of the Alech Hills

Our knowledge of the Alech Hills geology is essentially limited to brief early accounts based on mapping by the Geological Survey of India (Fedden 1884; Bandopadhyaya 1976). A few subsequent studies have addressed the geochemistry and petrogenesis of the Alech silicic rocks (Maithani et al. 1995; Banerjee et al. 2007; Cucciniello et al. 2019). All these studies, however, lack a stratigraphic and physical volcanological framework that we present here. Figure 2a is a geological map combining Bandopadhyaya's (1976) and our own field observations, and Fig. 2b an interpretative cross section along a NW–SE profile line. All localities mentioned in this paper are marked in Figs. 1a, b and 2a, all mentioned elevations are above mean sea level, and numbers refer to both samples and outcrops. Our scientific terminology follows Bull and McPhie (2007), Knott et al. (2016), and Sheikh et al. (2020a, b).

The study area (Fig. 2a) is low-lying with a regional slope toward the south; part of the area is a forest reserve with entry restrictions. The Alech Hills, while reaching 298 m elevation in the northeast, are generally much lower (Figs. 2a, 3, 4a). The hills are mostly composed of silicic volcanic rocks, and they have a distinctly arcuate shape and concentric-annular arrangement which controls the

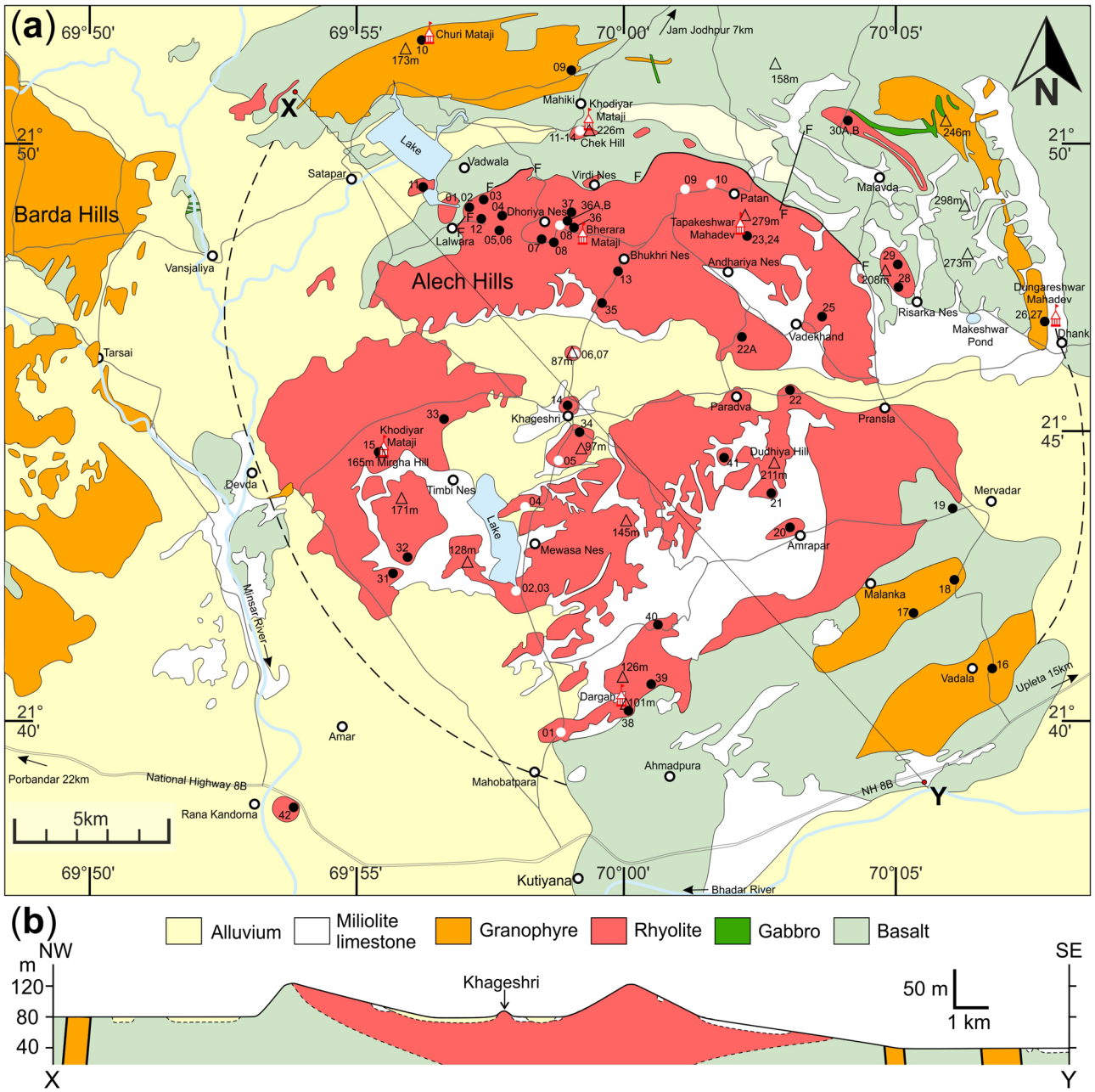

Fig. 2 **a** Geological map of the Alech Hills and a part of the Barda Hills to the west, based on Bandopadhyaya (1976) and our own field observations (in 2006, 2011, 2019, and 2020). The arcuate fault marked F–F in the northern part is as mapped by Bandopadhyaya (1976), and the dashed line represents the probable continuation of the granophyre ring dyke under the younger cover. Open triangles show elevations in meters above sea level, and locality names with suffixes "Mataji", "Mahadev" and "Dargah" are shrines. "Nes" refers to shepherds' hamlets. Wavy light blue lines are rivers and grey lines are roads. N.H.8B is National Highway 8B. White dots represent our 14 samples collected in 2019 along an essentially N–S traverse between Kutiyana and Jam Jodhpur (numbered AL19/01 to AL19/14), and black dots represent 42 additional samples collected in 2020 from all over the Alech Hills (numbered AL20/01 to AL20/42). The prefix "AL" has been removed from the sample numbers shown on the map to avoid cluttering. **b** NW–SE cross-section of the Alech Hills along line X–Y shown in **a**. Vertical exaggeration is 22X. Dashed lines indicate inferred or plausible contact geometries

major drainage lines. The village of Khageshri at ~ 75 m elevation forms the geographic center of the Alech Hills, and the north-convex arcs of rhyolite hills to the north of Khageshri have greater relief and continuity compared to the south-convex arc of rhyolite hills to the south of it (Figs. 2a, 3). The low country outside the outermost ring of hills and the depressions between the hills expose the basaltic lavas, and the Quaternary-age Miliolite limestone

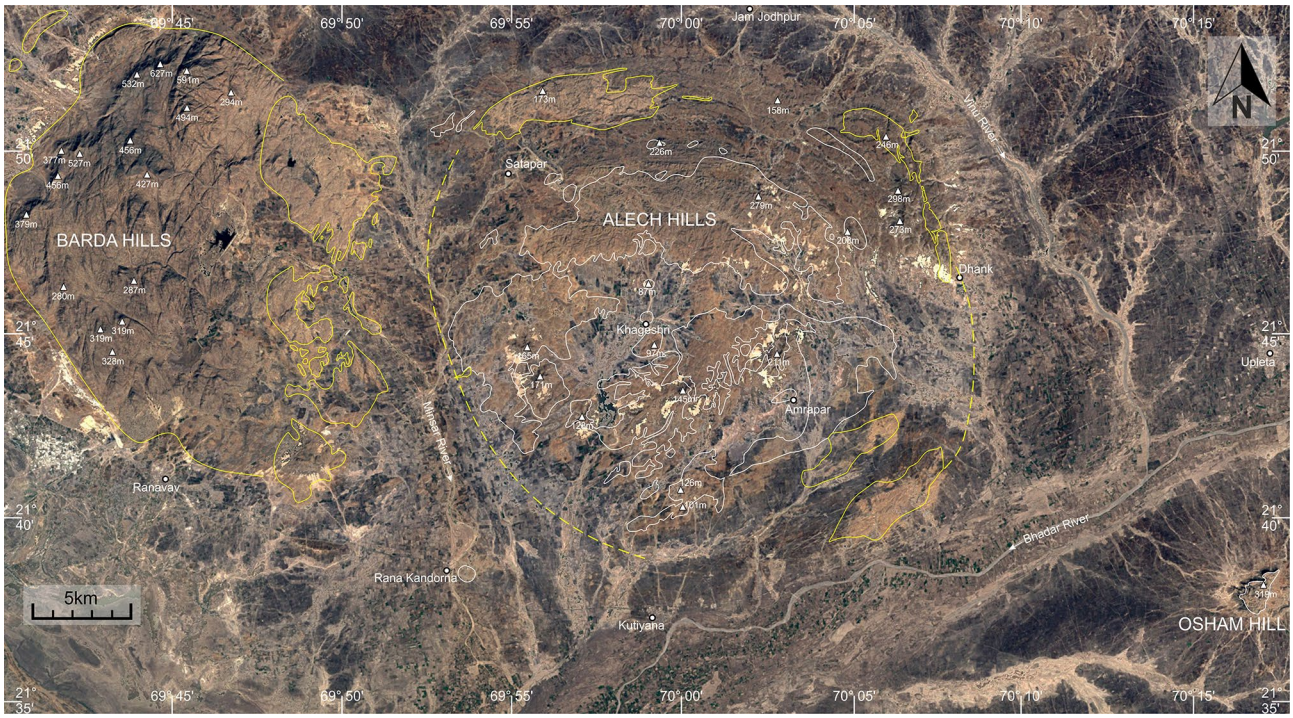

Fig. 3 Satellite image (courtesy Google Earth) of the Alech Hills, the Barda Hills to the west, and the Osham Hill to the southeast, in which the topographic and the most important geological elements have been superimposed. Areas enclosed by yellow lines are granophyres, including the Barda Hills granophyres and the Alech Hills ring dyke. Areas enclosed by white lines are rhyolites of the Alech Hills described in this paper. The Osham Hill is a small but important outcrop of rheomorphic and lava-like ignimbrites (Sheikh et al. 2020a; Naik et al. 2021)

and alluvium. The Miliolite limestone composed of tests of Miliolid foraminifera is widespread in Saurashtra. It has been interpreted as formed by shallow marine deposition (Shrivastava 1968; Lele 1973) or aeolian transport of calcareous beach sands to the inland areas (Biswas 1971). The Miliolite limestone is often found at considerable elevations, for example, at ~ 193 m at Tapakeshwar Mahadev Temple, where it forms 15–20 m thick cross-bedded sequences filling valleys in the eroded rhyolites. It is exposed at ~ 75 m around Khageshri.

A compound pāhoehoe basaltic lava flow forms the Vinu River bed 5 km east of Dhank (Fig. 4b). Mafic-looking rock outcrops mapped as basalt by Bandopadhyaya (1976), such as AL19/11 at the base of Chek Hill (226 m) or AL20/19 near Mervadar, show little or no calcic plagioclase but an abundance of alkali feldspar under the microscope, implying that parts of the geological map in Fig. 2a may be in need of revision. A huge ring dyke of granophyre, with a diameter of 30 km as measured in a NW–SE direction, intrudes the basaltic lava flows. Its exposure is not continuous because of widespread limestone and alluvium cover, and its estimated diameter as measured in a NE–SW direction is 26.5 km (Fig. 2a). The ring dyke has characteristic bouldery topography (Fig. 4c), homogeneous outcrop appearance without internal structures and megacrysts and a medium grain size (Fig. 4d). It shows characteristic granophyric intergrowths between quartz and alkali feldspar under the microscope (Fig. 4e, f). Fayalitic olivine, opaque oxides and zircon are present as accessory minerals, and weathering is evident from the state of the olivine and many alkali feldspar grains and the presence of secondary calcite (Fig. 4g). The ring dyke is distinct from the numerous granophyre intrusions which compose the Barda Hills (627 m) on the west (Dave 1971; De and Bhattacharya 1971; Cucciniello et al. 2019) (Fig. 3). The Barda plutonic complex was emplaced over a few million years, as indicated by $^{40}Ar/^{39}Ar$ ages of 69–68 Ma on three of the granophyre intrusions (Cucciniello et al. 2019) and zircon U–Pb ages of 66–65 Ma on others (Basu et al. 2020). We consider the south-flowing Minsar River (Figs. 2a, 3) as the geographic boundary between the Alech and the Barda Hills.

Silicic volcanic units overlie the basaltic lavas within the circular area bounded by the granophyre ring dyke, but are nowhere found in contact with the granophyre (Fig. 2a). Table 1 presents major oxide data for some of these silicic rocks (Cucciniello et al. 2019); mineral chemical and whole-rock trace element and Sr–Nd isotopic data are also provided in that study. Five of the analyzed samples are rhyolites and two are dacites. The rocks are weakly to strongly peraluminous, with up to 12 wt.% normative corundum as determined using the SINCLAS program (Verma et al.

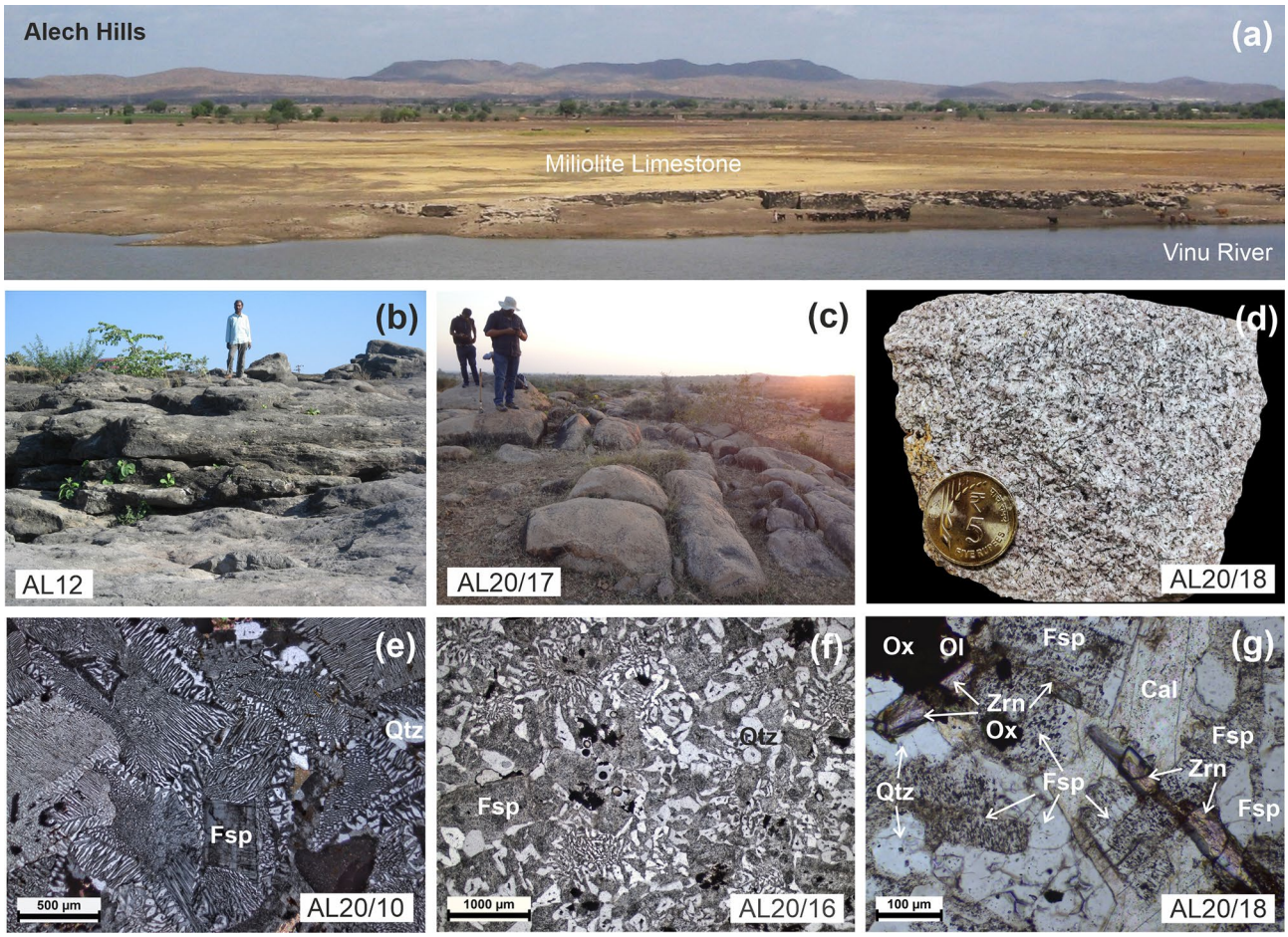

Fig. 4 Geological features of the Alech Hills. **a** Typical scenery of the Alech Hills, here looking west-northwest from a dam on the Vinu River 5 km east of Dhank. Shepherd with goat herd on the river bank provides an approximate scale. **b** Compound pāhoehoe basaltic lava flow (sample AL12 of Cucciniello et al. 2019) on the bank of the Vinu River, 5 km east of Dhank. **c** Flat topography and bouldery outcrops of the granophyre ring dyke southeast of Malanka (AL20/17). **d** Hand specimen photograph of the granophyre AL20/18 east of Malanka. Coin is 2 cm in diameter. **e** Thin section photomicrograph, in cross-polarised light (xpl), of granophyric intergrowths between alkali feldspar (Fsp) and quartz (Qtz) in granophyre AL20/10 at Churi Mataji temple. **f** Photomicrograph in plane-polarised light (ppl) of granophyric intergrowths in granophyre AL20/16 east of Vadala. **g** Photomicrograph (ppl) of accessory minerals in granophyre AL20/18. Mineral name abbreviations used are: *Fsp* alkali feldspar; *Qtz* quartz; *Ol* olivine; *Ox* Fe-Ti oxides; *Zrn* zircon; *Cal* calcite

2002). GPS-based coordinates of all the outcrops and samples mentioned in this study, and their elevations above mean sea level (with an uncertainty of ± 3 m), are provided in Table 2.

The Alech rhyolites: facies and morphotypes

Grey porphyritic rhyolite

The oldest exposed rhyolitic unit in the Alech Hills is a grey, moderately feldspar-phyric rhyolite (Fig. 5a) which is everywhere weathered to a characteristic golden brown color (Fig. 5b–e). It is also characteristically columnar-jointed at most outcrop locations. At the water plant hill south of Mewasa Nes (Fig. 5b), the rhyolite shows sub-vertical joints trending N40°, N135°, and N190°, and also sub-horizontal joints spaced centimeters to tens of centimeters apart which strike N350° and dip 10° due N260°. Columnar joints at the location in Fig. 5e show plumose markings and form two prominent sets with a strike of N17° and dip of 85° due west and a strike of N350° and dip of 70° due east. The near-verticality of the columnar joints in the rhyolite at numerous locations suggests that the unit is essentially horizontal over its wide outcrop area.

The grey porphyritic rhyolite shows no rheomorphic features (flow banding or folding). It shows considerable hydrothermal alteration at places, reflected in manganese dendrites (Fig. 5d), and particularly in the widespread

Table 1 Major oxide data and CIPW norms for the Alech Hills silicic rocks

	AL20/42	AL19/03	AL19/01	AL20/37	AL19/05	AL19/12,13	AL19/14
	AL1	AL4	AL5	AL7	AL3	AL10	AL11
	Grey porphyritic	Grey porphyritic	Red rheomorphic	Red rheomorphic	Tuff	Tuff	Dyke in tuff
Name	Rhyolite	Rhyolite	Rhyolite	Dacite	Rhyolite	Rhyolite	Dacite
SiO_2	69.82	71.29	77.28	66.53	86.71	77.72	65.60
TiO_2	0.35	0.34	1.02	0.78	0.24	0.73	1.12
Al_2O_3	13.97	13.30	12.88	12.24	7.03	10.43	11.42
Fe_2O_{3T}	3.63	4.43	1.85	8.87	1.03	4.40	11.47
MnO	0.03	0.09	0.05	0.16	0.01	0.01	0.12
MgO	0.13	0.07	0.08	0.21	0.03	0.11	0.22
CaO	0.21	0.36	0.28	1.96	0.22	0.13	0.38
Na_2O	3.91	4.39	0.06	2.94	0.03	0.03	0.75
K_2O	4.96	4.77	1.04	3.26	0.11	0.55	4.29
P_2O_5	0.01	0.02	0.04	0.20	0.02	0.15	0.21
LOI	2.06	1.01	5.51	3.26	3.44	4.94	4.83
Total	99.08	100.07	100.08	100.41	98.87	99.20	100.42
Mg No	9.31	4.35	11.1	6.01	7.62	6.70	4.91
Q	27.13	25.40	76.57	30.50	89.57	78.81	42.02
Or	30.29	28.54	6.51	19.96	0.68	3.46	26.76
Ab	34.18	37.61	0.54	25.78	0.26	0.27	6.70
An	1.01	1.67	1.19	8.72	1.01	–	0.54
C	1.87	0.31	11.90	0.82	6.83	10.41	5.65
Hy	3.11	3.74	0.26	8.67	0.63	3.16	10.92
Mt	1.69	2.02	0.88	3.53	0.49	2.11	4.64
Il	0.69	0.65	2.05	1.53	0.48	1.48	2.24
Ap	0.02	0.05	0.10	0.48	0.05	0.24	0.51

Notes: the data are from Cucciniello et al. (2019). Numbers in boldface are sample numbers of this study; corresponding sample numbers (ALxx) in the study of Cucciniello et al. (2019) are shown. AL1 is AL20/42 (grey porphyritic rhyolite at Rana Kandorna), AL3 is AL19/05 (silicified tuff from southwestern part of 97 m mound), AL4 is AL19/03 (grey porphyritic rhyolite at the base of water plant hill in Fig. 5b), AL5 is AL19/01 (red rheomorphic rhyolite north of Mahobatpara), AL6 is AL19/06 (tuff from 87 m mound north of Khageshri), AL7 is AL20/37 (red rheomorphic dacite between Dhoriya Nes and Bherara Mataji), AL10 is AL19/12 and AL19/13 (Chek Hill tuff), and AL11 is AL19/14 (dacite dyke intruding Chek Hill tuff). The major oxide values and CIPW normative minerals (in italics) are in weight percent. The CIPW norms, Mg number values, and rock names based on the total alkali-silica diagram were computed with the SINCLAS program (Verma et al. 2002). Fe_2O_{3T} = total iron expressed as Fe_2O_3; Mg number = 100 $Mg^{2+}/(Mg^{2+} + Fe^{2+})$, atomic

development of Liesegang rings (Liesegang 1907; Fig. 5e). The grey porphyritic rhyolite has very uniform petrographic features throughout its extent, with euhedral phenocrysts of alkali feldspar dispersed in a well-crystallised groundmass of quartz and alkali feldspar. Pyroclasts or vitroclasts are absent. Two representative thin-section photomicrographs are shown in Fig. 5f, g.

Near Rana Kandorna village, ~ 10 km from the southern limit of the Alech rhyolites (Fig. 2a), a small rhyolite inlier surrounded by alluvium is encountered at ~ 30 m elevation. This rhyolite inlier (AL20/42) has a gently domal topography and sub-horizontal exfoliation jointing in contrast to the tabular form and common columnar jointing of the grey porphyritic rhyolite. It is similar to the grey porphyritic rhyolite petrographically (Fig. 5h) and geochemically (sample AL1 of Cucciniello et al. 2019). As reported in that study, phenocrysts in the grey porphyritic rhyolite are anorthoclase ($An_{12-3}Ab_{71-63}Or_{17-34}$) and groundmass alkali feldspars range from $An_2Ab_{60}Or_{38}$ to $An_1Ab_{50}Or_{49}$. The rhyolite has 70–71 wt.% SiO_2, low TiO_2 (0.34–0.35 wt.%), and high to very high concentrations of the incompatible elements (Nb 108 ppm, Zr 584–610 ppm, Y 106–109 ppm, and Ba 1259–1782 ppm). It is weakly peraluminous with up to 2 wt.% normative corundum (Table 1).

A map of the grey porphyritic rhyolite (Fig. 6) yields a minimum preserved surface area of ~ 95 km^2, measured by overlaying a 1 × 1 km grid. Its thickness is more uncertain, as its base is not exposed anywhere and its top has been eroded. The rhyolite has an exposed thickness of ~ 20 m in the water plant hill (Fig. 5b), but is thicker (~ 40 m) at Mirgha Hill. A similar thickness is apparent from the difference in elevation between the northern outcrops AL20/11 and

Table 2 GPS coordinates of the outcrops and samples mentioned in the study, with the major eruptive units arranged in the order of younging stratigraphic position upwards

Number	Rock unit	Latitude	Longitude	Elevation (m)
AL19/07	Rhyolitic dykelets	N 21° 46′ 21.6″	E 69° 58′ 55.6″	87 m
AL19/14	Dacite dyke	N 21° 50′ 11.9″	E 69° 59′ 12.7″	197 m
AL20/42	Grey porphyritic rhyolite plug	N 21° 38′ 36.3”	E 69° 53′45.8”	33 m
AL20/10	Granophyre ring dyke	N 21° 51′ 46.4″	E 69° 56′ 05.0″	121 m
AL20/16	Granophyre ring dyke	N 21° 40′ 54.6″	E 70° 06′ 36.9″	53 m
AL20/17	Granophyre ring dyke	N 21° 41′ 52.1″	E 70° 05′ 08.4″	63 m
AL20/18	Granophyre ring dyke	N 21° 42′ 26.0″	E 70° 05′ 55.1″	67 m
AL20/27	Granophyre ring dyke	N 21° 46′ 55.1″	E 70° 07′ 35.4″	135 m
AL19/05	Tuff	N 21° 44′ 33.1″	E 69° 58′ 36.7″	87 m
AL19/06	Tuff	N 21° 46′ 21.6″	E 69° 58′ 55.6″	87 m
AL19/12	Tuff	N 21° 50′ 11.2″	E 69° 59′ 08.8″	226 m
AL19/13	Tuff	N 21° 50′ 11.5″	E 69° 59′ 09.7″	220 m
AL20/30	Tuff	N 21° 50′ 25.8″	E 70° 03′ 50.4″	135 m
AL20/34	Tuff	N 21° 45′ 01.2″	E 69° 59′ 00.0″	85 m
AL20/36	Tuff	N 21° 48′ 31.3″	E 69° 58′ 53.2″	114 m
AL20/36B	Tuff	N 21° 48′ 35.8″	E 69° 58′ 52.2″	120 m
AL19/04	Breccia (collapse breccia)	N 21° 43′ 43.4″	E 69° 58′ 00.3″	71 m
AL20/29	Breccia	N 21° 47′ 50.8″	E 70° 04′ 52.1″	173 m
AL20/14	Crystal-rich ignimbrite	N 21° 45′ 28.3″	E 69° 58′ 47.6″	88 m
AL20/06	Eutaxitic ignimbrite	N 21° 48′ 30.5″	E 69° 57′ 30.1″	123 m
AL20/07	Eutaxitic ignimbrite	N 21° 48′ 16.8”	E 69° 58′ 9.0”	114 m
AL20/12	Eutaxitic to parataxitic-rheomorphic ignimbrite	N 21° 48′ 39.9″	E 69° 57′ 12.5″	110 m
AL20/25	Eutaxitic to parataxitic-rheomorphic	N 21° 46′ 58.6″	E 70° 03′ 27.8″	123 m
AL19/01	Rheomorphic rhyolite	N 21° 39′ 49.8″	E 69° 58′ 39.4″	60 m
AL19/09	Rheomorphic rhyolite	N 21° 49′ 07.0″	E 70° 00′ 55.7″	149 m
AL20/01	Rheomorphic rhyolite	N 21° 48′ 52.6″	E 69° 56′ 58.3″	98 m
AL20/04	Rheomorphic rhyolite	N 21° 48′ 39.9″	E 69° 57′ 33.2″	124 m
AL20/08	Rheomorphic rhyolite	N 21° 48′ 16.6″	E 69° 58′ 31.3″	111 m
AL20/20	Rheomorphic rhyolite	N 21° 43′ 21.6″	E 70° 02′ 54.3″	66 m
AL20/22	Rheomorphic rhyolite	N 21° 45′ 42.9″	E 70° 02′ 52.5″	85 m
AL20/36A	Rheomorphic dacite	N 21° 48′ 35.7″	E 69° 58′ 53.2″	110 m
AL20/37	Rheomorphic dacite	N 21° 48′ 43.3″	E 69° 58′ 51.0″	104 m
AL20/38	Rheomorphic rhyolite	N 21° 40′ 12.9″	E 69° 59′ 54.6″	70 m
AL20/39	Rheomorphic rhyolite	N 21° 40′ 41.0″	E 70° 00′ 19.5″	69 m
AL19/02	Grey porphyritic rhyolite lava	N 21° 42′ 16.4″	E 69° 57′ 45.9″	67 m
AL19/03	Grey porphyritic rhyolite lava	N 21° 42′ 14.4″	E 69° 57′ 53.3″	55 m
AL19/08	Grey porphyritic rhyolite lava	N 21° 48′ 32.6″	E 69° 58′ 39.1″	117 m
AL20/11	Grey porphyritic rhyolite lava	N 21° 49′ 10.7”	E 69° 56′06.6”	89 m
AL20/15	Grey porphyritic rhyolite lava	N 21° 44′ 40.8”	E 69° 55′03.8”	135 m
AL20/21	Grey porphyritic rhyolite lava	N 21° 43′ 58.6”	E 70° 02′ 3.0”	96 m
AL20/22A	Grey porphyritic rhyolite lava	N 21° 46′ 38.1″	E 70° 01′ 56.8″	124 m
AL20/41	Grey porphyritic rhyolite lava	N 21° 44′ 30.8”	E 70° 01′40.4”	100 m

AL20/28 (Fig. 6). Assuming a minimum original thickness of 40 m, and given the rhyolite's essential horizontality over the whole area, we compute a minimum original volume of 3.8 km^3 for this rhyolite.

Rheomorphic rhyolites

Rheomorphic rhyolites are encountered at several places in the area, showing flow banding and flow folding on a range

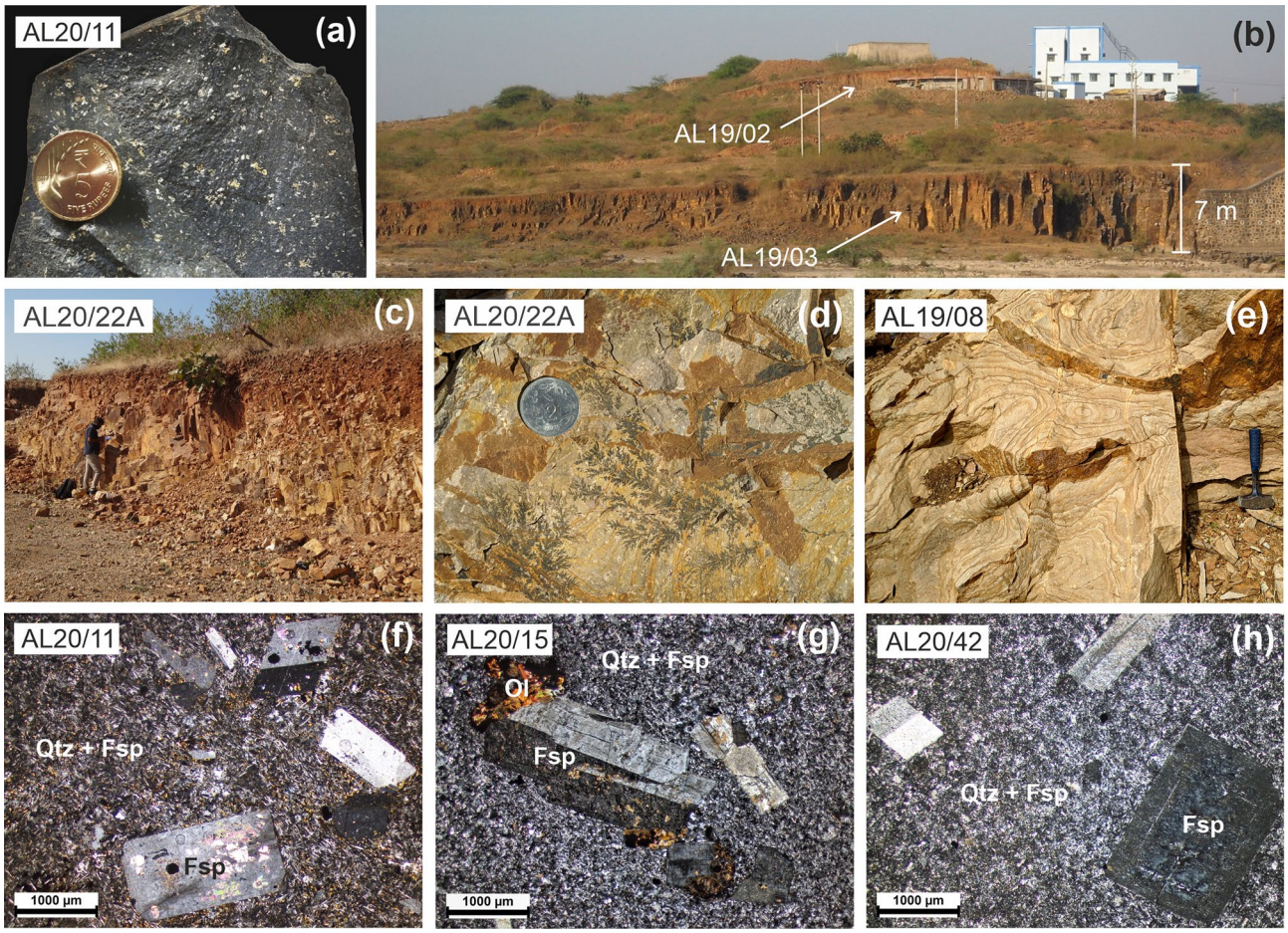

Fig. 5 Outcrop features of the grey porphyritic rhyolite which is everywhere weathered to a golden brown color. **a** Fresh surface of the grey porphyritic rhyolite AL20/11 east of Satapar. Coin is 2 cm wide. **b** Columnar-jointed outcrop in the water plant hill south of Mewasa Nes (samples AL19/02,03). **c** Columnar-jointed outcrop between Paradva and Vadekhand (AL20/22A). **d** Manganese dendrites on a joint face of the rhyolite AL20/22A. Coin is 2.5 cm wide. **e** Extensive development of Liesegang rings in the rhyolite outcrop AL19/08 southwest of Dhoriya Nes and west of Bherara Mataji. Blasted rock face in front is horizontal, and the face behind the 28 cm long hammer is vertical. **f**, **g** Photomicrographs (xpl) of samples AL20/11 collected near Satapar and AL20/15 from Mirgha Hill, showing the typical and uniform petrographic appearance of the grey porphyritic rhyolite. *Fsp* is feldspar, *Qtz* quartz, and *Ol* olivine (altered). **h** Similar petrographic appearance of the rhyolite AL20/42 at Rana Kandorna in the south

of scales from tens of meters to microscopic scale (Fig. 7). These overlie the grey porphyritic rhyolite, as inferred from their systematically higher elevations within a given area, though sections showing stratigraphic relationships are rare.

In the northern Alech Hills, a cluster of rheomorphic rhyolites is found between Lalwara, Dhoriya Nes and Bherara Mataji, and includes the outcrops AL20/01, AL20/04, AL20/08, AL20/12, AL20/36A, and AL20/37 (Figs. 2a, 6). Rheomorphic rhyolite AL19/09 west of Patan also possibly belongs to this cluster. Rhyolite AL20/37 shows large-scale, gently folded flow banding (Fig. 7a). Rhyolites AL20/01 and AL20/04 show meters scale and intricate, centimeter- to microscopic-scale flow folds (Fig. 7b–d). Rhyolite AL20/08 shows sheath folds in outcrop with two generations of flow folds under the microscope that produce a Type-3 interference pattern (Ramsay 1967) (Fig. 7e). Rhyolite AL20/22 shows flow banding and folding on the scale of the hand specimen. In thin section, it shows dark, fine-grained and light-colored microcrystalline flow bands wrapped around euhedral feldspar phenocrysts (Fig. 7f).

In the southern Alech Hills, rheomorphic deformation of rhyolite AL20/20 at Amrapar has produced a diverse and complex set of flow folds, some of which are interpreted as refolded F_1 folds with a Type-2 fold interference pattern (Ramsay 1967) (Fig. 7g). Pucker lineations are observed on some of these fold surfaces. Outcrop AL20/39 north of Ahmadpura (Fig. 7h) shows gradations from eutaxitic to parataxitic and highly rheomorphic textures. It is also characterised by numerous highly stretched vesicles forming partings along flow bands and spectacular Type-3 fold interference patterns (Fig. 7i). Outcrop AL20/25 near Vadekhand, dominantly parataxitic with tight small-scale

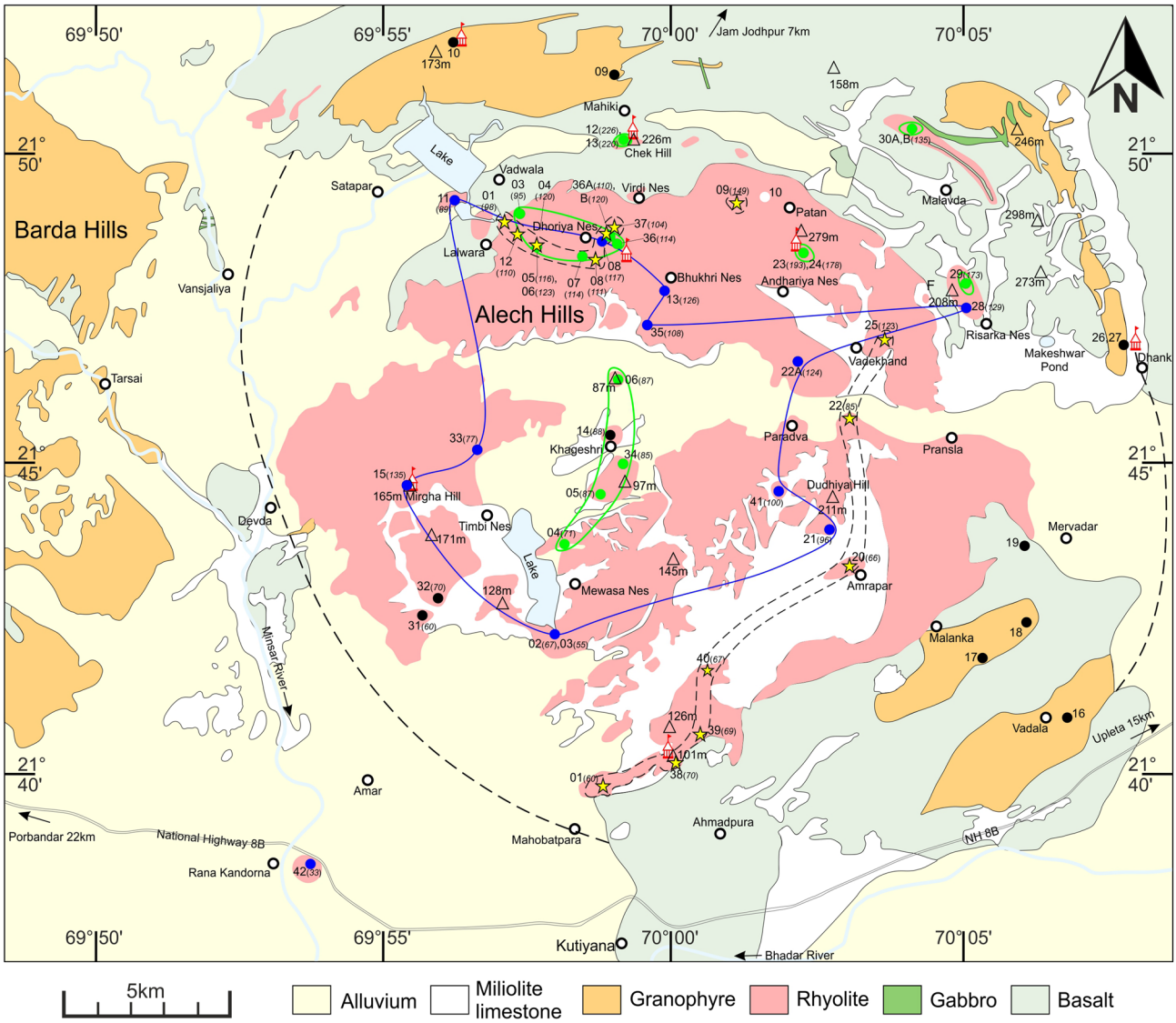

Fig. 6 Geological map showing the Alech rhyolites distinguished by facies, against a somewhat faded background of the rock types as shown in Fig. 2a. Dark blue dots are the outcrops of grey porphyritic lava, whose outcrop area is enclosed by the dark blue line, and also the Rana Kandorna rhyolite inlier (possibly a plug). Yellow stars indicate rheomorphic and eutaxitic ignimbrites, with outcrop areas enclosed by the dashed black lines. Green dots are massive tuffs and breccias, with outcrop areas enclosed by green lines. For each type and outcrop, sample number is indicated in upright font and the sample elevation (in meters above mean sea level) is indicated in italicised font within brackets, so as to facilitate an understanding of the eruptive stratigraphy as discussed in the text

flow folds, also shows parts which are eutaxitic, with pumice fiamme. Outcrop AL19/01 north of Mahobatpara shows flow layering which strikes N325° and dips 22° due N235°, and a flow lineation plunging 18° due N272°. Some rheomorphic rhyolite outcrops, such as AL20/04, AL20/38 and AL20/39, show well-formed, sub-vertical columnar joints in parts.

Interestingly, the rheomorphic rhyolites mentioned above (AL19/01, AL19/09, AL20/04, AL20/08, AL20/20, AL20/25, AL20/36A, AL20/37, and AL20/39) are all red to dark brown, though they are not necessarily the same eruptive unit. Thus AL20/37 (Fig. 7a) is a dacite with ~ 67 wt.% SiO_2 and ~ 9 wt.% total iron, whereas AL19/01 is a high-silica rhyolite with > 77 wt.% SiO_2 and only ~ 2 wt.% total iron (Table 1). Figure 6 shows the areal distribution of the rheomorphic (and the overlying eutaxitic) rhyolites as observed by us. Of all the rheomorphic rhyolites shown in Fig. 7, only AL20/04 shows well-identifiable vitroclasts, highly stretched and folded, in thin section (Fig. 7d).

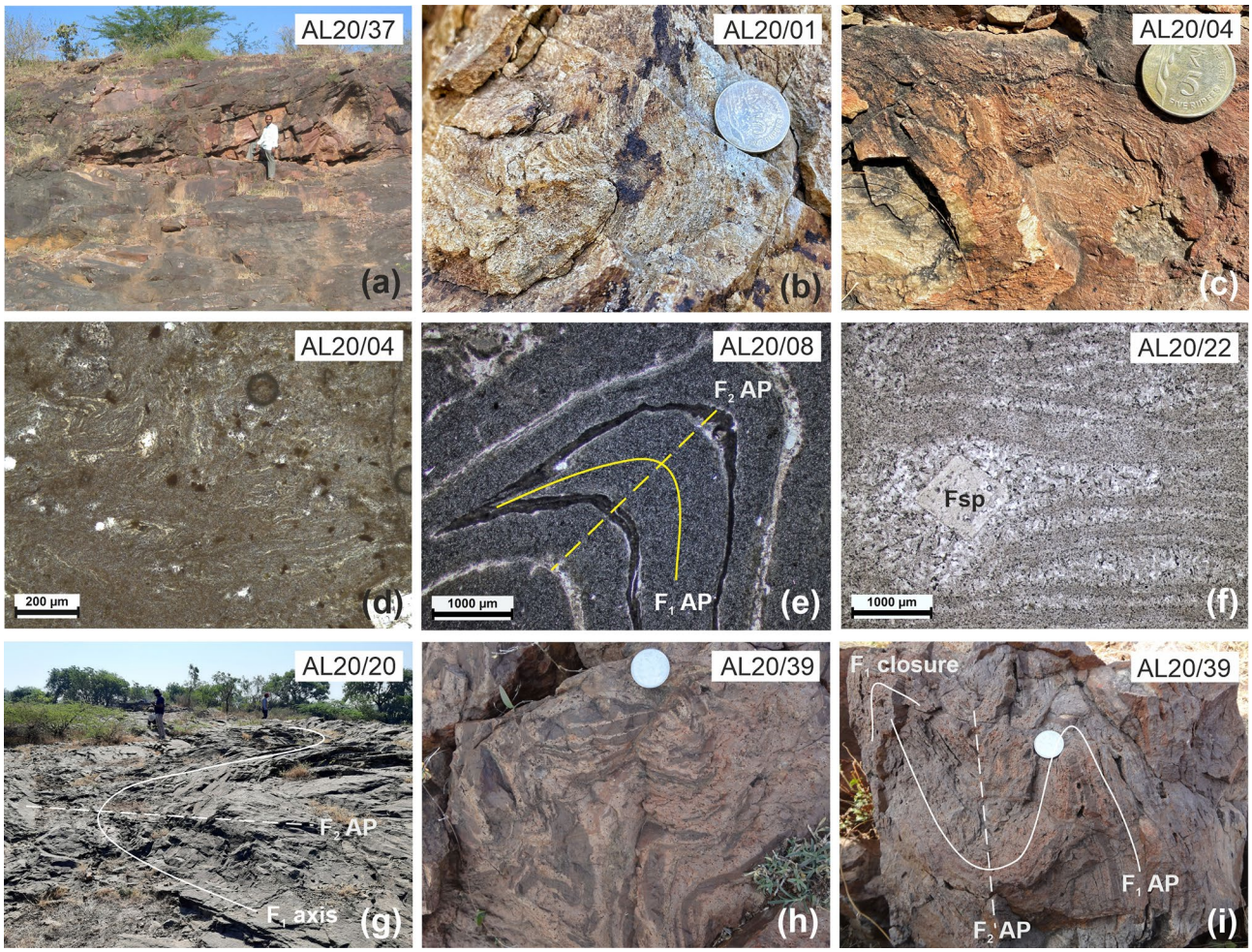

Fig. 7 Rheomorphic rhyolites in the Alech Hills. **a** Large-scale, gently folded flow layering in rhyolite AL20/37 northeast of Dhoriya Nes. **b** Small-scale folds in rhyolite AL20/01 northeast of Lalwara. Coin is 2 cm wide. **c** Close-up of outcrop of rhyolite AL20/04 between Lalwara and Dhoriya Nes, showing exquisite small-scale folding and refolding. Coin is 2 cm in diameter. **d** Photomicrograph (xpl) of rhyolite AL20/04 showing highly stretched and folded vitroclasts. Bubbles are not vesicles but air bubbles introduced during sample preparation owing to the porous nature of the rock. **e** Photomicrograph (ppl) showing two phases of folding (F_1 and F_2) in the rhyolite AL20/08 south of Dhoriya Nes. AP denotes trace of axial plane. **f** Photomicrograph (ppl) of rhyolite AL20/22 between Paradva and Pransla, showing well-developed flow banding (including microcrystalline bands) wrapped around a euhedral feldspar (Fsp) crystal. **g** Refolded F_1 folds producing a Type-2 fold interference pattern in rhyolite AL20/20 northwest of Amrapar village; persons for scale. **h** Folded fiamme in rhyolite AL20/39 north of Ahmadpura. Subhorizontal outcrop face, coin 2.5 cm wide. **i** Refolded F_1 fold showing hook-shaped, Type-3 fold interference pattern in AL20/39. Note abundant stretched vesicles along flow bands and partings. Subhorizontal outcrop face, coin 2.5 cm wide

Eutaxitic ignimbrites

There is good field evidence that the eutaxitic ignimbrites (Fig. 8) stratigraphically overlie the rheomorphic rhyolites. For example, in the northern areas, the eutaxitic ignimbrite outcrop AL20/06 (Fig. 8a–c) fills saddles in the undulating upper surface of rheomorphic rhyolite AL20/04 (Fig. 7c, d). In parts of the former outcrop, the pumice fiamme are elongated but randomly oriented (Fig. 8a), grading laterally into horizontally elongated and dark fiamme, whereas the opposite face of the same outcrop shown in Fig. 8a shows highly elongated, dark fiamme, some with gentle folding or warping (Fig. 8b, c). Rhyolite AL20/25 near Vadekhand shows flow banding and folding and relict pumice fiamme which have been rotated to sub-vertical during rheomorphic flow, with their cross sections exposed on horizontal rock faces (Fig. 8d). This outcrop shows small-scale features suggestive of elutriation pipes (Fig. 8e). White tuff with fiamme (AL20/07) is also found south of Dhoriya Nes.

Some houses in the village of Khageshri have been constructed from blocks of eutaxitic ignimbrite with the distinctive dark pumice fiamme (Fig. 8f). An old abandoned fort at the center of the village sits on a mound ~ 15 m high but with no rock exposures. The dark green, highly

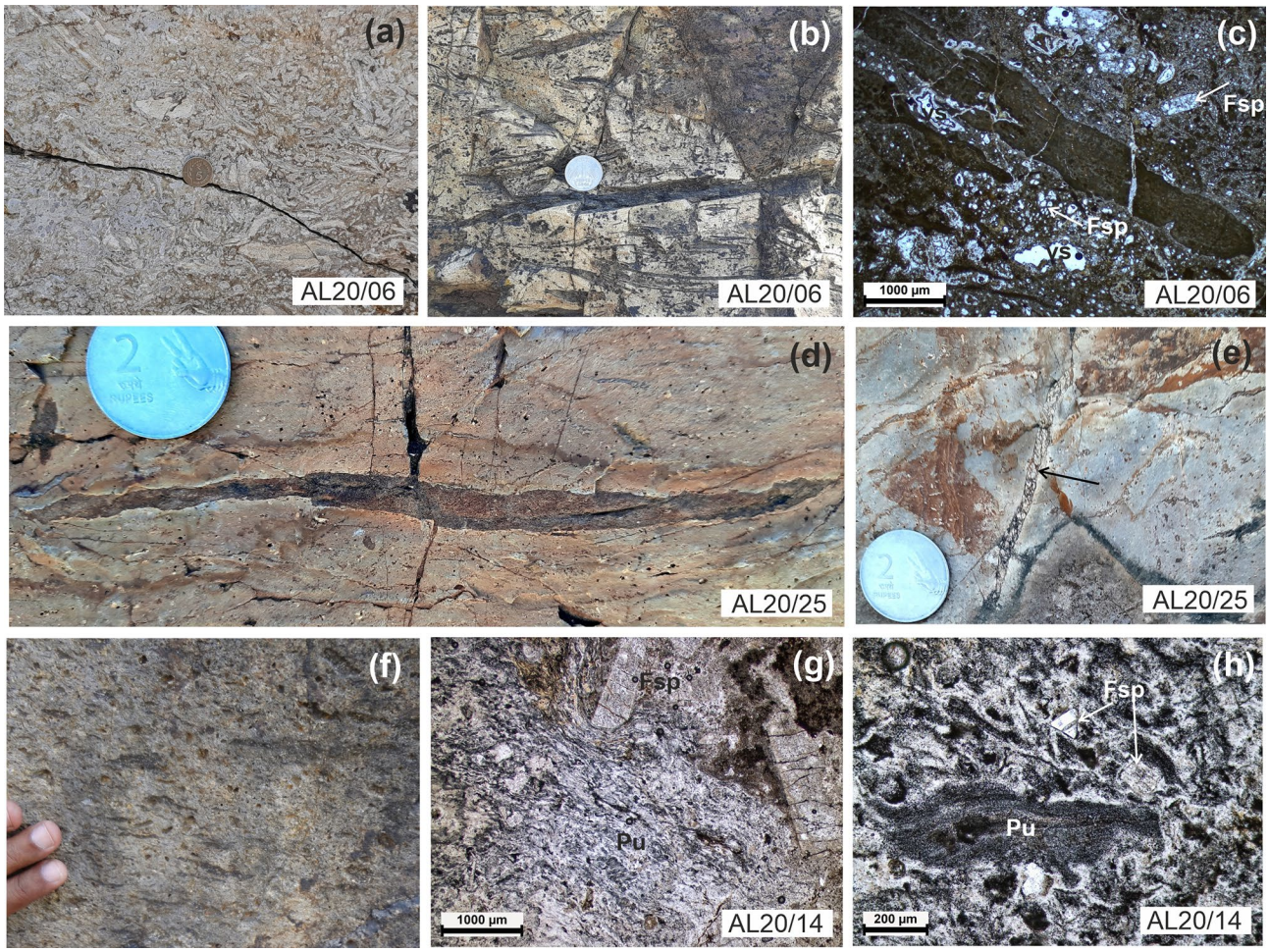

Fig. 8 Eutaxitic ignimbrites in the Alech Hills. **a** Elongated white pumice fiamme which do not show a preferred orientation, in ignimbrite AL20/06 east of Lalwara. Vertical outcrop face, coin 2 cm wide. **b** Dark, small to large pumice fiamme, highly vertically compressed and horizontally stretched (and some folded) on the opposite side of the outcrop face shown in (**a**). Coin is 2.5 cm wide. **c** Thin section photomicrograph (ppl) of AL20/06, showing fiamme, feldspar crystals (Fsp) and vesicles (vs). **d** Large, gently folded pumice fiamma with numerous smaller, subparallel fiamme in ignimbrite AL20/25 east of Vadekhand. Plan view of sub-horizontal outcrop face (foliation sub-vertical), coin 2.5 cm wide. **e** Possible elutriation pipe (marked by black arrow) in ignimbrite AL20/25, sub-horizontal face, coin 2.5 cm wide. **f** Block of eutaxitic ignimbrite used in house wall at Khageshri. Dark pumice fiamme are distinct; apparent stretched vesicles are parts where weathering has removed original fiamme. The "brecciated and mylonitised feldspathic rocks" of Banerjee et al. (2007) may actually have been such ignimbrites. **g** Photomicrograph (ppl) of rhyolite AL20/14 exposed outside Khageshri fort, showing a large fragment of fibrous pumice (Pu) wrapped around a feldspar (Fsp) crystal, with numerous adjacent feldspar crystals. **h** Photomicrograph (ppl) of AL20/14 showing a dark, fibrous pumice fragment in a matrix of devitrified pumice and glass shards with a few feldspar crystals

porphyritic rock AL20/14 exposed outside the fort gate contains darker fiamme, and may be the rock described by Bandopadhyaya (1976) as a sodic rhyolite with phenocrysts of sanidine and some anorthoclase. The rock is a crystal-rich ignimbrite in which the fibrous pumice fiamme are wrapped around feldspar crystals (Fig. 8g). The pumice fiamme show varying degrees of compaction (Fig. 8g, h).

Tuffs and breccias

The eutaxitic ignimbrites are in turn overlain by non-welded tuffs and breccias which lack structures such as bedding, size sorting, or grading. As seen around Bherara Mataji, these tuffs and breccias (outcrops AL20/36 and AL20/36B at 114 m) overlie rheomorphic units (such as AL20/36A and AL20/37). Breccia outcrop AL20/29 showing ferruginisation forms much of the 208 m hill south of Malavda, and directly overlies the basalts (Fig. 9a). Tuffs of rhyolitic composition (Table 1) form most of the 226 m Chek Hill. Massive tuffs

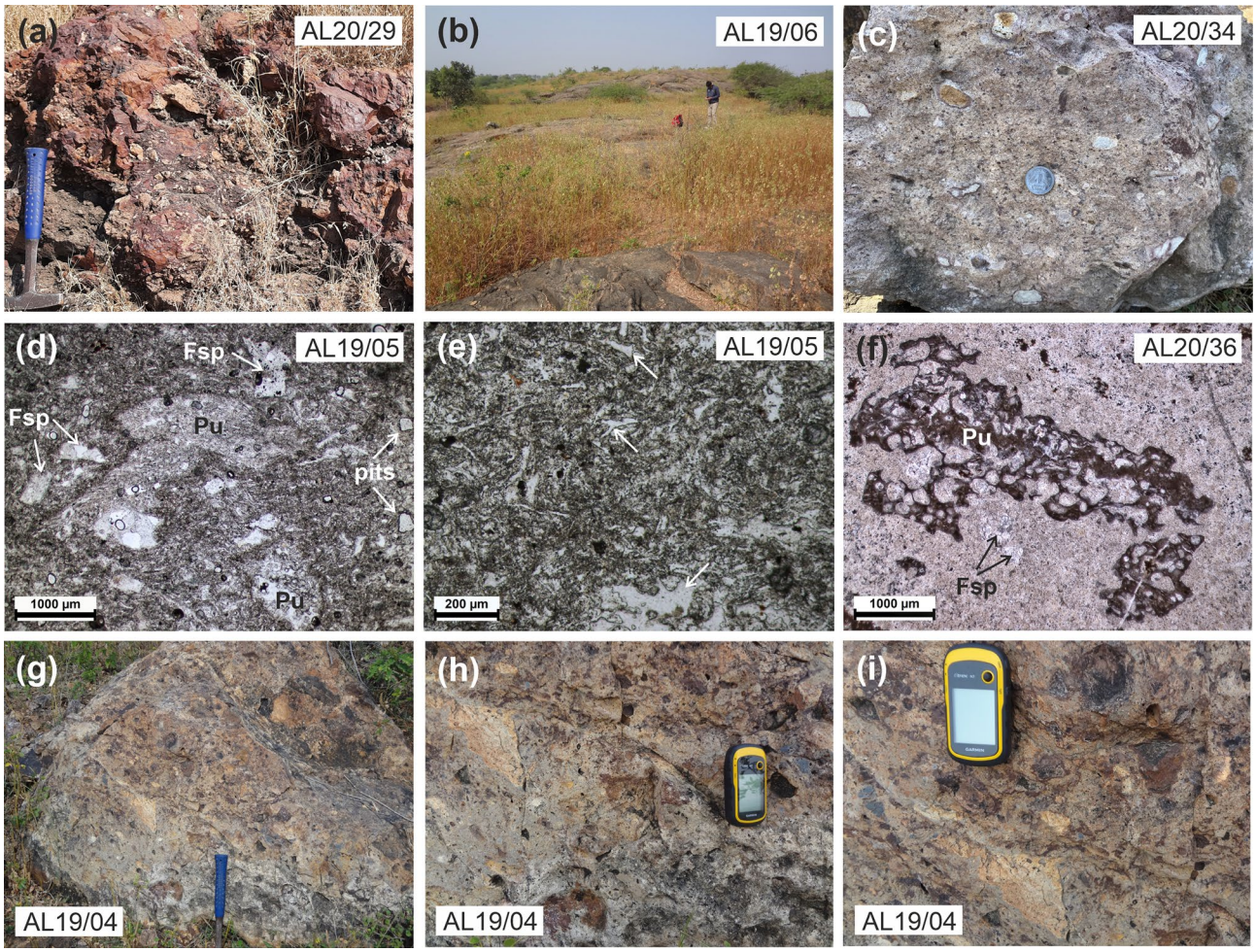

Fig. 9 Tuffs and breccias in the Alech Hills. **a** Ferruginised massive breccia forming the 208 m hill in the northeastern Alech Hills. Hammer is 33 cm long. **b** Extensive outcrops of massive tuff AL19/06 forming the 87 m mound 2 km north of Khageshri village. **c** Tuff AL20/34 at the southern end of Khageshri village. Coin is 2.5 cm wide. **d**, **e** Photomicrographs (ppl) of tuff AL19/05 south of Khageshri. Devitrified fibrous pumice fragments (Pu) and bubble-wall shards including Y-shaped shards (some indicated by white arrows) are present, along with some feldspar (Fsp) crystals. Note air bubbles and pits related to sample preparation. **f** Photomicrograph (ppl) of a dark pumice fragment in breccia AL20/36 near Bherara Mataji, contained within a devitrified matrix of ash with a few feldspar (Fsp) crystals. **g** Massive breccia AL19/04 (possible caldera-collapse mesobreccia) forming a low mound north of Mewasa Nes. Hammer is 33 cm long and vertical. **h**, **i** Close-up views of breccia AL19/04, with GPS for scale

are exposed over an extensive low-lying area (~ 85 m) around Khageshri, such as tuff AL19/05, AL19/06 (Fig. 9b) and AL20/34 (Fig. 9c). Tuff AL19/05 is cut by sub-vertical joints striking N40°, N270° and N320°, whereas tuff AL19/06 is traversed by orthogonal joints, one set striking N50° (with a dip of 87° due NW) and the other striking N140° (with a dip of 75° due NE). Spectacular Liesegang rings are observed in fine-grained tuffs AL20/30 near Malavda. A small outcrop of bedded tuffs occurs near the water plant hill of the grey porphyritic rhyolite, at location N 21° 42′ 17.7″, E 69° 57′ 47.6″, 64 m. The tuffs have a strike N285° and dip 23° due N20°, i.e., toward Khageshri.

In thin section, the tuff AL19/05 shows fragments of devitrified fibrous pumice and feldspar crystals (Fig. 9d), and bubble-wall glass shards that range from cuspate to Y-shaped (Fig. 9e). The breccia AL20/36 shows highly vesicular glass shards in a matrix of ash (Fig. 9f).

An ~ 25 m high, elongated mound located west of the road from Mewasa Nes to Khageshri, with its base at 71 m, is composed of massive tuff breccias (AL19/04, Fig. 2a). These contain centimeter- to decimeter-sized clasts of rhyolite in a fine-grained ash matrix (Fig. 9g–i). The rock is matrix-supported to clast-supported, and the angular to sub-rounded clasts range in color from light yellow and shades of brown to nearly black glassy rhyolitic types. Some of the individual clasts are distinctly composed of several smaller clasts and are thus composite.

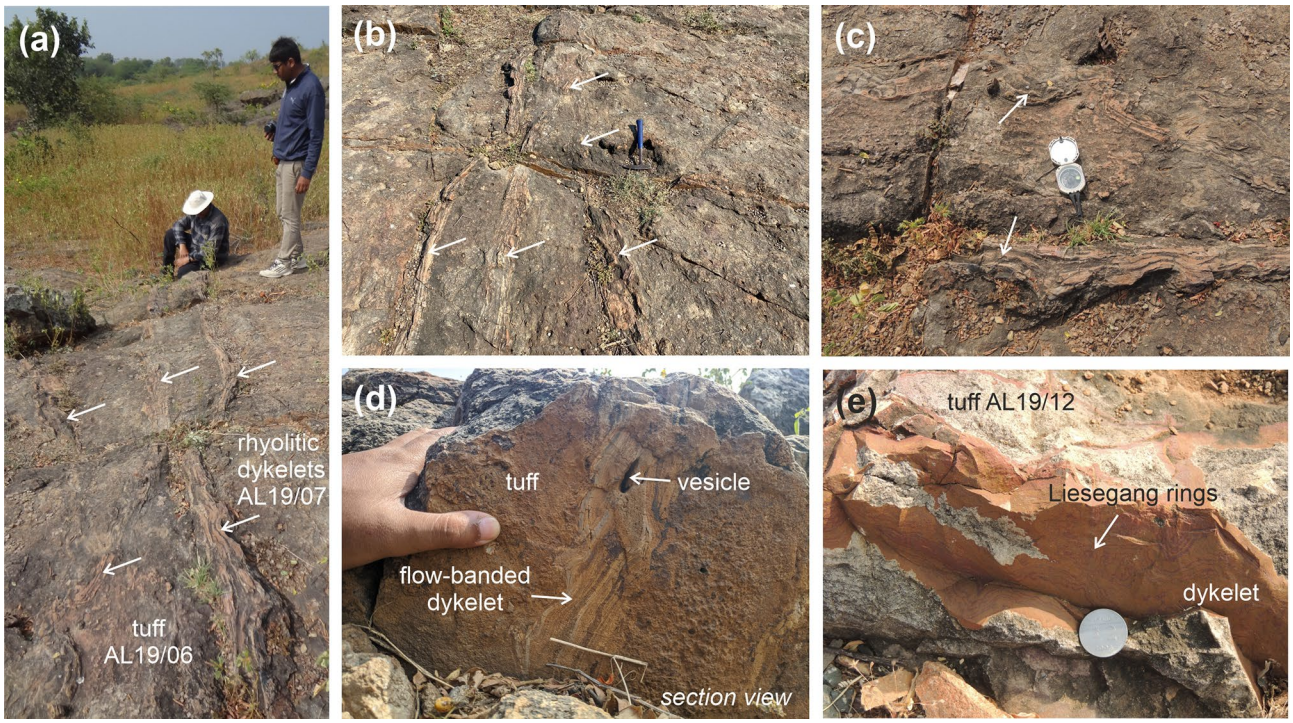

Fig. 10 Rhyolitic intrusions in the Alech Hills tuffs and breccias. **a–d** Rhyolite dykelets (AL19/07, marked by white arrows) intruding massive tuff AL19/06 in the 87 m mound 2 km north of Khageshri. Panels (**b**, **c**) are oblique plan views, whereas panel (**d**) is a vertical profile view. Note orthogonal joint sets in (**b**). **e** One of a few dykelets of red rhyolite intruding massive tuff AL19/12 at the 226 m summit of Chek Hill. Coin is 2.5 cm wide

Rhyolitic intrusions

The massive tuffs found south of Khageshri (AL19/05 and AL20/34) also form the 87 m mound 2 km north of the village (outcrop AL19/06, Figs. 2a, 9c). The tuff here is intruded by numerous rhyolite dykelets (AL19/07) a few meters in exposed length and several centimeters wide (Fig. 10a–c). The dykelets trend along several directions, merge and splay. Individual dykelets show prominent deflections in plain view (Fig. 10c) that reflect changing rock stiffnesses and local stresses (Gudmundsson et al. 2010). Cross-sectional views of the dykelets reveal vertical flow layering and flow folding, as well as vesicles stretched vertically (Fig. 10d). A distinct margin-parallel surface lineation on the dykelets (Fig. 10a–c) is thus revealed to be the trace of the vertical flow layering. Thin sections reveal the individual flow bands to be as thin as 50 µm and up to a few hundred µm thick.

A dark grey glassy dacite dyke (AL19/14, Table 1) intrudes the rhyolitic tuffs of Chek Hill (226 m) at 197 m elevation, whereas the same tuffs at the 226 m summit of the hill show centimeters-thick dykelets of red rhyolite (Fig. 10e), some showing Liesegang rings.

Rhyolite dykes exposed south of Dhoriya Nes hamlet have yielded extremely high concentrations of Nb (up to 1000 ppm), Zr (> 1000 ppm), La (up to 251 ppm) and Y (up to 337 ppm) (Maithani et al. 1995). Cucciniello et al. (2019) found 852 ppm Nb, 291 ppm Y, 254 ppm La, and 2650 ppm Zr in their dyke AL9 from this location. The huge granophyre ring dyke has already been mentioned. Bandopadhyaya (1976) also mentioned a banded rhyolite dyke near Malavda which trends NW–SE (parallel to the granophyre ring dyke), and gabbro and dolerite dykes near Malavda and Virdi Nes (Fig. 2a).

A summary of the outcrop and textural features and mineral assemblages of the Alech rhyolites described above is provided in the Table 3, along with their physical volcanological interpretations (see below).

Discussion

Physical volcanological interpretations of the Alech rhyolites

Rheomorphic deformation features (flow banding and folding) are common in both rhyolitic lavas and high-grade to extremely high-grade, lava-like ignimbrites (e.g., Lenhardt et al. 2017; Sheikh et al. 2020a, b; Naik et al. 2021). The grey porphyritic rhyolite (Fig. 5) lacks these features. Basal

Table 3 Summary table of physical and textural characteristics of the Alech Hills silicic rocks

Unit	Thickness and location	Outcrop features and structures	Constituents and textures	Interpretation
Intrusions	Centimeters to meters; mostly central and northern parts	Granophyre ring dyke up to 5 km wide and with a diameter of 30 km; rhyolitic dykelets with flow banding, doleritic and gabbroic dykes	Quartz and alkali feldspar, accessory zircon, with variable amounts of glass	Ring dyke marks outer boundary fault, other intrusions may mark caldera resurgence
Tuffs and breccias	Meters; central and northern parts	Mostly massive (without bedding, size grading, cross-bedding or other structures) and non-welded	Pumice fragments and glass shards, and some feldspar crystals, in a matrix of ash, commonly devitrified; breccias with abundant lithic fragments of rhyolite in ash matrix	Non-welded, low-grade ignimbrites, some possible caldera-collapse mesobreccias
Eutaxitic ignimbrites	Meters; northern, central and southern parts	White or dark pumice fiamme defining a eutaxitic foliation, sometimes gradational into parataxitic and rheomorphic ignimbrites, columnar-jointed in parts	Pumice fiamme in a matrix of pumice and glass shards with variable amounts of feldspar crystals	Medium-grade, moderately welded ignimbrites
Rheomorphic ignimbrites	Meters, tens of meters in outcrops AL20/04 and AL20/37; northern and eastern parts	Flow banding and flow folding of several types (including sheath folds) and at least two generations, sometimes gradational into eutaxitic ignimbrites, columnar-jointed in parts	Highly deformed vitroclasts, some feldspar crystals, abundant glass in the matrix	Extremely high-grade, intensely welded, lava-like ignimbrites
Grey porphyritic rhyolite	~40 m maximum exposed thickness; most extensive unit, all parts	Commonly with subvertical columnar jointing, extensive development of Liesegang rings in some outcrops, no flow banding or folding	Anorthoclase phenocrysts in a fine groundmass of K-feldspar (sanidine) and quartz, no pyroclasts or vitroclasts	Flood rhyolite lava (≥ 3.8 km^3) from effusive eruption

breccias and steep lava flow fronts fringed by breccias are typical of rhyolite lavas (Henry and Wolff 1992; Ellis et al. 2013), but neither is exposed in this rhyolite. Whereas broken crystals are not a diagnostic indicator of pyroclastic origin (Henry and Wolff 1992; Sheikh et al. 2020b), the unbroken phenocrysts in this rhyolite are consistent with, and suggest, a lava. Most important, the well-crystallised groundmass of the rhyolite and the absence of pyroclasts or vitroclasts in it throughout its entire areal extent (Fig. 6) indicate that it is a lava, produced by a voluminous (≥ 3.8 km^3) effusive eruption. The eruptive vent is unknown and unexposed, noting that we do not see the base of the rhyolite. Sheet-like flows of rhyolite are comparatively uncommon, and the grey porphyritic lava of the Alech Hills (and the 50 m thick, ≥ 5 km^3 rhyolite lava of Mount Pavagadh, Sheikh et al. 2020b), are such flood rhyolite lavas (terminology of Henry and Wolff 1992) in the Deccan Traps.

The eutaxitic ignimbrites (Fig. 8) are easy to identify as such, but the underlying rheomorphic rhyolites (Fig. 7) may represent lavas or lava-like ignimbrites. Rheomorphic rhyolite AL20/04 shows distinct vitroclasts, highly stretched and folded, in thin section (Fig. 7d). Vitroclasts are not obvious in the other rheomorphic rhyolites. It is known that the lava-like flow, intense welding, and devitrification of extremely high-grade ignimbrites often obscures the original vitroclastic textures, and extremely compacted, stretched, and recrystallised vitroclasts can mimic flow bands in rhyolite lavas (e.g., Andrews and Branney 2005; Sheikh et al. 2020a, b). It is therefore likely that flow bands in the rheomorphic rhyolites represent original vitroclasts. In particular the white, microcrystalline flow bands in rhyolite AL20/22 (Fig. 7f) may represent devitrified pumice. We therefore consider that the rheomorphic rhyolites (Fig. 7) are lava-like ignimbrites produced by high-temperature pyroclastic density currents (e.g., Ellis et al. 2013; Knott et al. 2016). The development of F_1 tight-isoclinal folds (Fig. 7i), outcrop-scale sheath folds as well as F_1 tight-isoclinal folds superimposed by F_2 folds producing Type-2 (Fig. 7g) and Type-3 (Fig. 7e, i) interference patterns, all without the formation of penetrative axial planar cleavage, indicate dynamic and heterogeneous non-coaxial progressive ductile deformation during flow of the hot ignimbrites (see also Sheikh et al. 2020a; Naik et al. 2021).

The overlying eutaxitic ignimbrites (Fig. 8) were also produced by pyroclastic density currents (e.g., Ross and Smith 1961; Bull and McPhie 2007). The lava-like ignimbrites of the Alech Hills are comparable to those of Osham Hill in the immediate southeast (Fig. 3), and Snake River-type ignimbrites (Ellis et al. 2013; Sheikh et al. 2020a; Naik et al. 2021). The eutaxitic ignimbrites of the Alech Hills can also be compared to corresponding, albeit less common, examples in the Snake River Plain (Knott et al. 2016). In Saurashtra itself, eutaxitic ignimbrites have been described from Rajula (Krishnamacharlu 1974) and Bhaguda (Sheikh et al. 2020a), whereas Danian-age examples are found in the Mumbai area (Duraiswami et al. 2019).

The lava-like and eutaxitic ignimbrites are shown grouped together in Fig. 6. It is to be noted that outcrops, such as AL20/39 north of Ahmadpura (Fig. 7h, i) and AL20/25 near Vadekhand (Fig. 8d, e), show both types over lateral distances of meters to tens of meters, arguably owing to local differences in temperature and degree of welding. The eutaxitic ignimbrites stratigraphically above the rheomorphic ignimbrites may represent deposition from relatively cool pyroclastic density currents, or they may alternatively represent the faster-cooled and less intensely welded upper levels of the lava-like ignimbrites which did not participate in rheomorphic flow. The rare elutriation pipes (Fig. 8e), which indicate flushing of fine ash-charged vapors out of the cooling, degassing ignimbrite (Fisher and Schmincke 1984), are observed only in the lower-grade parts of the ignimbrites, implying that they were destroyed in the higher-grade ignimbrites. Put another way, elutriation pipes are not common because the ignimbrites are at least moderately welded.

The above inference regarding ignimbrite welding intensity and stratigraphic height also helps to understand why the massive tuffs such as AL19/05 forming the uppermost exposed parts of the eruptive sequence are non-welded (Fig. 9d). Cuspate and Y-shaped glass shards in the tuff AL19/05 (Fig. 9e) represent broken walls and junctions of adjacent gas bubbles, and indicate magmatic volatile-driven explosive fragmentation of magma rising in a conduit and experiencing decompression (e.g., Heiken 1974; Fisher and Schmincke 1984). The tuff AL19/05 with abundant pumice, feldspar crystals, and cuspate glass shards (Fig. 9d, e) closely resembles the non-welded, crystal-bearing, glass- and pumice-rich ash beds at Mount Pavagadh, interpreted by Sheikh et al. (2020b) as a thick primary fallout ash succession derived from distal Plinian eruptions, possibly in Saurashtra. Dark pumice fragments preserved in the breccia AL20/36 show abundant sub-spherical (some polygonal) and nearly touching vesicles (Fig. 9f). Such pumice represents a stage when the rhyolitic melt was essentially a bubbly foam, just before bubble-wall shard formation.

The absence of erosional surfaces or paleosols within the whole Alech rhyolitic sequence indicates rapid aggradation, beginning with a flood rhyolite lava from an effusive eruption and continuing with a series of pyroclastic density currents depositing hot ash and pumice that underwent decreasing degrees of loading compaction and rheomorphic deformation with stratigraphic height. The absence of sedimentary interbeds or peperites suggests a subaerial depositional environment (see also Naik et al. 2021).

Evidence for the Alech Hills as a giant silicic caldera

Bandopadhyaya (1976) mapped an arcuate ring fault in the rhyolites north of Lalwara, Dhoriya Nes and Patan (Fig. 2a) and, despite poor exposure, considered the fault as vertical or outward-dipping with a southward downthrow. He considered the granophyre ring dyke to fill a ring fracture which formed as a corollary to the subsidence. Based on these features and the radial-inward dips of the basaltic and rhyolitic units, the "crushed" nature of the uppermost rhyolites, and the volcanic breccias and vent-like features, he suggested central subsidence in a cauldron-like structure (e.g., Clough et al. 1909 for the Silurian-age Glencoe silicic caldera in Scotland). Cucciniello et al. (2019), noting volcanic tuff and rheomorphically deformed rhyolites, considered that the Alech rhyolites may represent large-scale ring-fracture lavas and lava-like ignimbrites akin to those erupted from calderas in the Snake River Plain (e.g., Ellis et al. 2013; Knott et al. 2016).

Calderas have been defined as "large collapse depressions, more or less circular or cirque-like in form, the diameter of which is many times greater than any included vent" (Williams and McBirney 1979). We consider that the following features of the Alech Hills geology indicate, and are consistent with, a true volcanic caldera:

(i) The arcuate and annular geometry of the Alech Hills (Figs. 2a, 3) reflects structural control by ring faults, as observed by Bandopadhyaya (1976). He also noted that the rhyolitic units show gentle radial dips toward the central low area around Khageshri; note the cuesta form of the rhyolitic hills in Fig. 3.

(ii) The low elevation and relief of the Alech Hills are as expected for calderas, which are large volcano-tectonic depressions in the surrounding landscape (e.g., Williams and McBirney 1979; Lipman 2000; Cole et al. 2005; Branney and Acocella 2015).

(iii) There is the theoretical possibility and expectation that silicic calderas should occur in the Deccan Traps, noting that other CFB provinces contain them. In the Columbia River CFB province and the Snake River-Yellowstone "hotspot" track, rhyolites (both lavas and ignimbrites) erupted from calderas locally exceed the flood basalt volumes (e.g., Ellis et al. 2013; Knott et al. 2016). There are silicic calderas in the Scottish Hebridean CFB province, such as the Loch Bà caldera on Mull (Emeleus and Bell 2001), and in the Etendeka CFB province of Namibia, such as the Messum and Brandberg granitic ring complexes (Korn and Martin 1954; Milner et al. 1992; Schmitt et al. 2000).

(iv) The boundaries of silicic calderas of the world (whether formed in CFB provinces or arc settings) are often marked by ring dykes. Examples are the rhyolitic Loch Bà ring dyke, which is 8 km in diameter and up to 400 m wide (Emeleus and Bell 2001). Other examples are the Messum and Brandberg granitic ring dykes mentioned above, the many Jurassic-age (~ 160 Ma) Younger Granite ring intrusions in Nigeria and Niger (Wright 1985), and the 35 km wide peralkaline granite ring dyke that bounds the Siwana caldera in the 750 Ma Malani rhyolite province of Rajasthan, northwestern India (Bhushan and Chandrasekaran 2002). Similarly, at Alech Hills, the 30 km-diameter granophyre ring dyke (Figs. 2a, 3, 4d) marks the bounding ring fault of a caldera and thus the outer limit of volcanotectonic subsidence.

(v) Several of the Nigerian Younger Granites contain rhyolites (including ignimbrites) preserved within the areas of cauldron subsidence (Wright 1985), as indeed does the Siwana granite ring (Bhushan and Chandrasekaran 2002). The effusive and explosive Alech rhyolitic volcanism recorded within the area bounded by the granophyre ring dyke (Figs. 2a, 3) represent the comparable, intra-caldera lava and pyroclastics.

(vi) The Alech Hills caldera had numerous individual eruptive vents, represented in prominent hills composed of tuffs and breccias, such as Chek Hill (226 m) and the 208 m peak south of Malavda. Chek Hill may be a large tuff cone. The pyroclastic materials erupted from such vents were likely widely dispersed outside the caldera boundary, but these *extra-caldera* deposits have been removed by erosion. Rhyolite AL20/42 at Rana Kandorna in the south, outside the granophyre ring, resembles the intra-caldera grey porphyritic lava in its petrographic and geochemical features but not outcrop features. This rhyolite may be a plug of the same magma emplaced along the caldera rim.

(vii) The silicic (and some mafic) intrusive activity within the rhyolitic volcanics of Alech Hills, including in the youngest erupted units (the nonwelded tuffs), may be related to post-collapse caldera resurgence. It is not known if these exposed intrusions fed further eruptions.

(viii) The fact that the Barda plutonic complex occupies substantially higher elevations (from sea level to 627 m), compared to the essentially volcanic Alech Hills (up to 298 m) (Fig. 3), strongly suggests large-scale subsidence of the latter consistent with a caldera. The amount of subsidence is not possible to determine because of the lack of any marker horizon which can be correlated within and outside the Alech Hills. However, the reasonable argument that the Alech rhyolites originally occupied higher structural levels than the Barda complex, and their current differences in elevation, together imply a structural subsidence of the Alech rhyolites by ~ 1 km.

(ix) Calderas contain caldera-collapse megabreccias and mesobreccias, derived by erosion of the steep fault scarps of the intra-caldera rhyolites (Lipman 1976). Some of the coarse breccias exposed around Khageshri (Fig. 9g–i), containing decimeter-sized angular fragments of rhyolites, may represent such mesobreccias. The composite large clasts in the breccias are consistent with formation by mass movements (sliding or avalanching) of originally deposited tuffs and breccias. The ash matrix of the composite breccias may also reflect grinding of the clasts during mass movements, and these mesobreccias have been subsequently cemented. We have not observed caldera-collapse megabreccias, which may be deeply buried under the intra-caldera Alech rhyolites.

(x) Many of the Alech rhyolites show extensive hydrothermal alteration and incompatible element (Nb, Zr, Y, La) enrichments (Maithani et al. 1995; Banerjee et al. 2007; Cucciniello et al. 2019). The grey porphyritic rhyolite (Fig. 5e) and several tuff outcrops (Fig. 10e) show Liesegang rings that reflect pervasive alteration. Secondary silicification has also occurred; for example, the tuff AL19/05 south of Khageshri has nearly 87 wt.% SiO_2 and 90 wt.% normative quartz (Table 1), values which cannot be magmatic. Widespread hydrothermal alteration and silicification are common features of calderas (e.g., Lipman 2000).

Whereas the above features of the Alech Hills taken singly may be inconclusive or circumstantial (e.g., the hydrothermal alteration), taken together, they provide strong evidence that the Alech Hills of Saurashtra represent a giant silicic caldera in the northwestern Deccan Traps CFB province.

Implications of the Alech Hills as a giant silicic caldera

Recognition of the Alech Hills as an eroded silicic caldera helps to understand several features of its geology. Gudmundsson (2015) finds that when a block of crust containing a shallow-level, sill-like magma chamber experiences doming by a deeper and much more areally extensive magmatic reservoir, tensile stresses are created at the surface that lead to caldera formation (Fig. 11a). The dominantly silicic magmas of the Alech Hills are consistent with pre-eruptive storage in one or more shallow-level magma chambers (e.g., Cashman and Giordano 2014; Weber and Castro 2017).

The low relief of the Alech Hills, and the absence of vertical sections (especially those perpendicular to the granophyre ring dyke strike) preclude a determination of the dip of the ring dyke. However, ring dykes are typically vertical or outward-dipping for the following reasons (Gudmundsson 2015, 2020). Where the caldera boundary ring fault dips steeply inward (a common scenario), the subsiding piston-type inner crustal block encounters friction along the fault walls as well as compression, often leading to its trapping before it reaches the shallow-level magma chamber. On the other hand, if the caldera boundary ring fault is vertical or steeply outward-dipping (Fig. 11b), the piston-like block can subside to greater depths (Fig. 11c, d) and collapse on the shallow-level magma chamber, leading to the emptying of much of the chamber via the ring fault (forming the ring dyke which feeds eruptions) (Fig. 11d, e). The magma reduces the friction on the fault walls, facilitating further subsidence. Note that in the case of a steeply outward-dipping caldera boundary fault, the gap between the subsiding piston and the host (filled by the ring dyke) becomes progressively wider as the piston subsides further (Gudmundsson 2015, 2020). The caldera ring fault along which the kilometer-wide Alech Hills ring dyke has been emplaced is thus highly likely to have been steeply outward-dipping.

Silicic ring dykes typically have a discontinuous outcrop (e.g., Fig. 30 of Emeleus and Bell 2001; Fig. 9 22 of Gudmundsson, 2020), and the Alech Hills granophyre ring dyke is no exception (Fig. 2a). The dyke is very likely to be present between its exposed segments under the widespread younger cover of limestone and alluvium (the dashed line in Figs. 2a, 3, 6), but is absent from the basalt outcrops in the north and the south. Its absence in these parts may be due to factors such an unfavourable crustal stress field or insufficient magma availability which prevented dyke emplacement altogether, or which led to dyke arrest below current exposure level (Gudmundsson 2020).

Calderas are divided into several types (plate or piston, downsag, piecemeal, or trapdoor calderas) based on the nature of the dominant tectonic movement, though it is well recognised that many calderas fit more than one of these endmember types (Lipman 2000; Cole et al. 2005; Acocella 2007; Branney and Acocella 2015). Glencoe, the type locality for cauldron subsidence or caldera collapse (Clough et al. 1909), has been reinterpreted as of piecemeal type (Moore and Kokelaar 1998).

At Alech Hills, the very wide and thick and nearly circular granophyre ring dyke suggests piston-type downward movement of a coherent (even if internally faulted) crustal block along a steeply outward-dipping (or vertical) ring fault and its collapse into a shallow-level silicic magma reservoir. Evidence for structural control of the arcuate-annular rhyolitic ridges (Bandopadhyaya 1976, Fig. 2a) also suggests intra-caldera faulting with a concentric plan form (Fig. 11e). Such extensional faulting of the progressively thickening intra-caldera rhyolite sequence can be related to periodic magma chamber recharge leading to caldera resurgence and

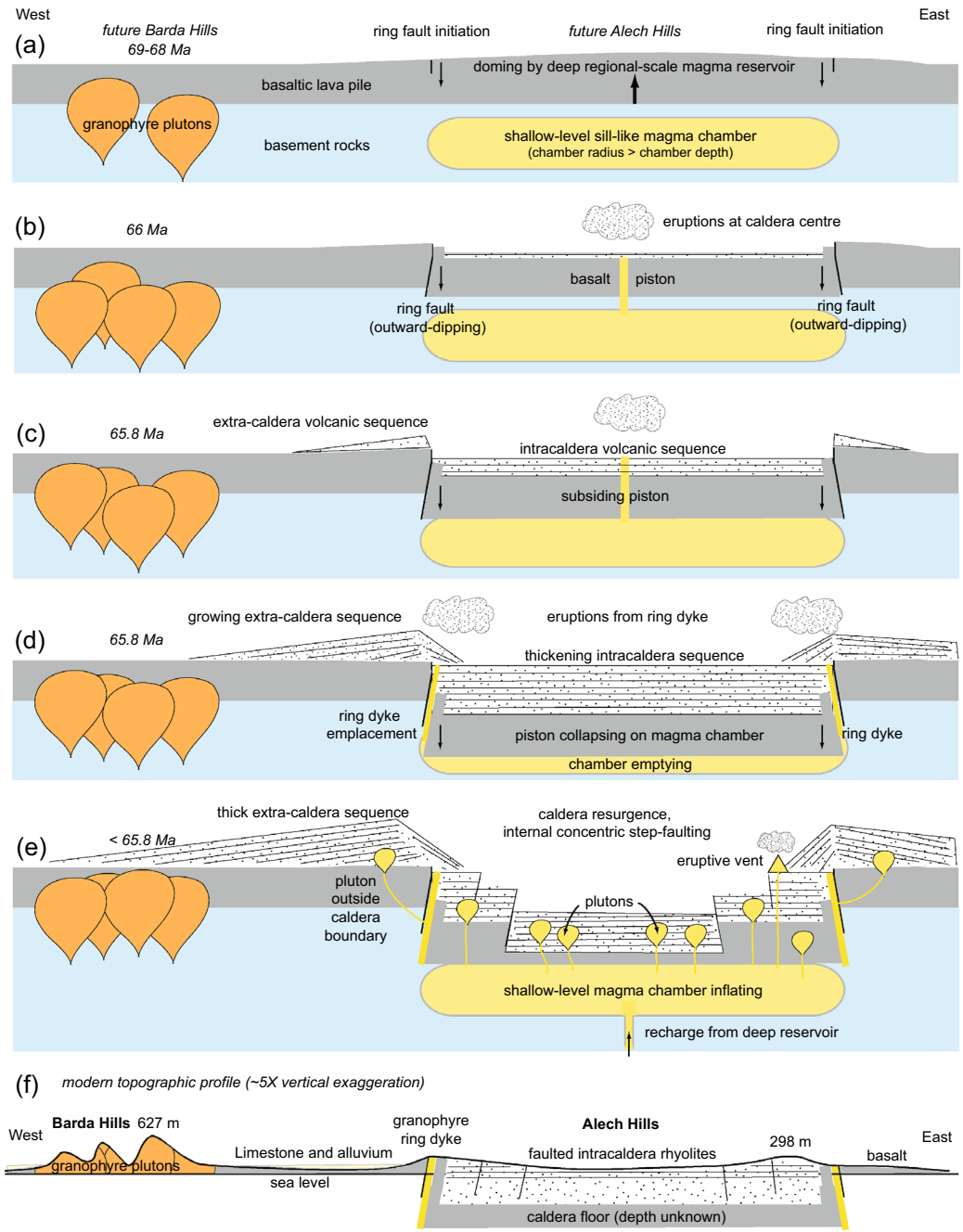

Fig. 11 a–f Cartoon schematically illustrating the stages of development of the Alech Hills caldera (see text). Cartoon is based on the limited geochronological data yet available for the Alech and Barda Hills (Cucciniello et al. 2019; Basu et al. 2020), and many cycles of caldera inflation and deflation connected with periodic magma recharge and eruptions are likely. The last panel depicts the modern topography and the distribution of the major rock units. The west-to-east distance and vertical exaggeration in each panel are ~ 45 km and ~ 5X, respectively

shallow-level magma intrusions. The extensional faulting would in turn facilitate new eruptions by decompression of shallow-level plutons or the gravitational collapse of fault blocks on them, all of these phenomena operating in concert with continuing periodic subsidence of the whole circular caldera block. We note that the non-welded tuffs and breccias crop out at high elevations in the Alech Hills (e.g., above ~ 200 m at Chek Hill, and above ~ 135 m in the 208 peak) but at low elevations (71–87 m) north of Ahmadpura and around Khageshri (Fig. 6). This suggests that the central low-lying area of the Alech Hills around Khageshri is also that of the maximum structural subsidence, with the eutaxitic

and rheomorphic ignimbrites and the grey porphyritic lava (as well as deeper intra-caldera eruptive units not exposed currently) buried in the subsurface and well below sea level.

A semantic issue is whether the Alech Hills are a caldera or a cauldron. Cauldrons mark a stage in which most of the volcanic products erupted during caldera collapse have been removed, and the older volcanic or sedimentary units below the caldera floor have been exposed (Cole et al. 2005). Still deeper (> 2 km) erosion exposes the magma chamber(s) beneath an inferred caldera structure, and these are called ring structures (Cole et al. 2005; Branney and Acocella 2015); classical examples are the ~ 160 Ma Younger Granites of Nigeria–Niger or the ~ 120 Ma Brandberg Granite of Namibia mentioned above. At Alech Hills, whereas considerable erosion has exposed the granophyre ring dyke in many parts (Fig. 11f), the silicic eruptive units are still preserved, and hence we use the term caldera.

The eruptive vent locations of the widespread rhyolites and dacites of the northwestern and northern Deccan Traps are unknown; the Alech Hills caldera is an important potential source area for some of them. Sheikh et al. (2020a, b) suggested that the northern–northwestern Deccan silicic volcanism, both effusive and explosive, may have played a significant role in the K/Pg boundary mass extinction. The Alech Hills caldera is even more significant in this regard. Geochronological work on the Alech Hills rocks is largely lacking, but the granophyre ring dyke sampled northeast of Satapar has yielded a CA-ID-TIMS $^{206}Pb/^{238}U$ date of 65.765 ± 0.018 Ma (2σ, Basu et al. 2020). The recognition of the Alech Hills as a giant (30 km-diameter) silicic caldera, with both effusive and explosive eruptions, is therefore of fundamental importance not only in physical volcanology of the Deccan Traps and CFB provinces, but also from the point of view of their environmental impact and the K/Pg boundary mass extinction.

Conclusions

As noted by Branney and Acocella (2015), many calderas of the world are yet to be discovered. The geology, physical volcanology and stratigraphy of the Alech Hills in Saurashtra, in the northwestern Deccan Traps, have been poorly known, with brief early geological accounts (Fedden 1884; Bandopadhyaya 1976) and a few later geochemical studies (Maithani et al. 1995; Banerjee et al. 2007; Cucciniello et al. 2019). In the present study, based on geological and textural descriptions and physical volcanological interpretations, we recognize the Alech Hills as a giant (30 km-diameter, 660 km^2) silicic caldera which had both effusive and explosive eruptions. The lowest and most extensive unit, a ≥ 3.8 km^3 feldspar-phyric grey rhyolite, is an uncommon flood rhyolite lava. Abundant explosive volcanism is recorded in the overlying lava-like and eutaxitic ignimbrites, tuffs, and breccias. All of these units constitute only a small remnant, after extensive erosion, of what must have existed originally (Fig. 11e, f).

The Alech Hills silicic caldera is important for understanding Deccan CFB volcanism, and even more so given the 65.765 ± 0.018 Ma (2σ) date recently obtained on the granophyre ring dyke, which suggests that the caldera formation overlapped with the K/Pg boundary mass extinction and may have substantially contributed to it. The significant recognition of the Alech Hills giant silicic caldera now having been made, future work should include detailed geological and geophysical mapping to understand its eruptive stratigraphy and structure and the emplacement mechanics of the ring dyke, and geochemical and geochronological work (e.g., U–Pb zircon geochronology) on our large sample set. These datasets will be important for assessing the eruptive duration and intensity, probable environmental impact, and economic potential of the Alech Hills silicic caldera, followed by detailed comparisons between the Alech Hills and the much better-studied silicic calderas of the world.

Acknowledgements Field work was supported by an Institution of Eminence (IoE) research grant (No. Dev. Scheme 6031, PFMS Scheme 3254) from the BHU to Alok Kumar (Principal Investigator, Collaborator: H. Sheth). A. Naik is supported by a PhD Research Fellowship of the Council of Scientific Research (CSIR), Government of India (File No. 09/087(0908)/2017-EMR-I). J. M. Sheikh is supported by a Malaviya Postdoctoral Fellowship of the BHU (IoE Scheme, Ref. No. IoE/MPDF/2020-21/14). We are grateful to Agust Gudmundsson for answering several queries related to caldera volcanotectonics, to journal reviewers Nils Lenhardt and Raymond Duraiswami for helpful comments which improved this manuscript, and to Wolf-Christian Dullo for his editorial handling.

References

Acocella V (2007) Understanding caldera structure and development: an overview of analogue models compared to natural calderas. Earth-Sci Rev 85:125–160

Andrews GDM, Branney MJ (2005) Folds, fabrics, and kinematic criteria in rheomorphic ignimbrites of the Snake River Plain, Idaho: insights into emplacement and flow. In: Pederson J, Dehler CM (eds) Interior western United States, vol 6. Geological Society of America, USA, pp 1–17. https://doi.org/10.1130/2005.fld006(15)

Ayalew D, Barbey P, Marty B, Reisberg L, Yirgu G, Pik R (2002) Source, genesis, and timing of giant ignimbrite deposits associated with Ethiopian continental flood basalts. Geochim Cosmochim Acta 66:1429–1448

Baksi AK (2014) The Deccan Trap—cretaceous-palaeogene boundary connection; new $^{40}Ar/^{39}Ar$ ages and critical assessment of existing argon data pertinent to this hypothesis. J Asian Earth Sci 84:9–23

Bandopadhyaya S (1976) Acid ring dykes and lava flows in Deccan Trap basalt, Alech Hills, Saurashtra, Gujarat. In: Prasad B, Manjrekar BS (eds) Proc Symp Deccan Trap & Bauxite. Geol Surv Ind Spec Publ 14, pp 158–163

Banerjee R, Gurjar R, Maithani PB (2007) Geochemical characters of rare metal and rare earth elements bearing late phase acid effusives of Alech Hills, Jamnagar and Junagarh Districts, Gujarat. Gondwana Geol Mag Spec 10:145–159

Basu AR, Chakrabarty P, Szymanowski D, Ibanez-Mejia M, Schoene B, Ghosh N, Georg RB (2020) Widespread silicic and alkaline magmatism synchronous with the Deccan flood basalts. India Earth Planet Sci Lett 552:116616. https://doi.org/10.1016/j.epsl.2020.116616

Bhushan SK, Chandrasekaran V (2002) Geology and geochemistry of the Magmatic rocks of the Malani igneous suite and Tertiary alkaline province of western Rajasthan. Geol Surv Ind Mem 126:179

Biswas SK (1971) The Miliolite rocks of Kutch and Kathiawar (western India). Sed Geol 5:147–164

Branney MJ, Acocella V (2015) Calderas. In: Sigurdsson H (ed) Encyclopedia of volcanoes, 2nd edn. Elsevier, pp 299–315

Bull KF, McPhie JM (2007) Fiamme textures in volcanic successions: flaming issues of definition and interpretation. J Volcanol Geotherm Res 164:205–216

Cashman KV, Giordano G (2014) Calderas and magma reservoirs. J Volcanol Geotherm Res 288:28–45

Cassidy M, Manga M, Cashman K, Bachmann B (2018) Controls on explosive-effusive volcanic eruption styles. Nat Comm 9:2839. https://doi.org/10.1038/s41467-018-05293-3

Clough CT, Maufe HB, Bailey EB (1909) The cauldron-subsidence of Glen Coe, and the associated igneous phenomena. Quat J Geol Soc Lond 65:611–678

Cole JW, Milner DM, Spinks KD (2005) Calderas and caldera structures: a review. Earth-Sci Rev 69:1–26

Cucciniello C, Choudhary AK, Pande K, Sheth H (2019) Mineralogy, geochemistry and ^{40}Ar-^{39}Ar geochronology of the Barda and Alech complexes, Saurashtra, northwestern Deccan Traps: early silicic magmas derived by flood basalt fractionation. Geol Mag 156:1668–1690

Dave SS (1971) The geology of the igneous complex of the Barda Hills, Saurashtra, Gujarat State (India). Bull Volcanol 35:619–632

De A, Bhattacharya D (1971) Phase-petrology with special reference to pyroxenes of the acid igneous complex of Barda Hills, western Saurashtra (Gujarat). Bull Volcanol 35:907–929

Duraiswami RA, Jutzeler M, Karve AV, Gadpallu P, Kale MG (2019) Subaqueous effusive and explosive phases of late Deccan volcanism: evidence from Mumbai Islands, India. Arab J Geosci 12:1–21

Ellis BS, Wolff JA, Boroughs S, Mark DF, Starkel WA, Bonnichsen B (2013) Rhyolitic volcanism of the central Snake River Plain: a review. Bull Volcanol 75:745. https://doi.org/10.1007/s00445-013-0745-y

Emeleus CH, Bell BR (2001) The Palaeogene volcanic districts of Scotland, 4th edn. British Geological Survey, Nottingham, p 212

Fedden F (1884) The geology of the Kathiawar peninsula in Gujarat. Geol Surv Ind Mem 21:73–136

Fisher RV, Schmincke H-U (1984) Pyroclastic rocks. Springer-Verlag, Berlin Heidelberg, p 472

Francis P (1983) Giant volcanic calderas. Sci Am 248:60–73

Gudmundsson A (2015) Collapse-driven large eruptions. J Volcanol Geotherm Res 304:1–10

Gudmundsson A (2020) Volcanotectonics: understanding the structure, deformation, and dynamics of volcanoes. Cambridge University Press, Cambridge, p 586

Gudmundsson A, Simmenes TH, Larsen B, Philipp SL (2010) Effects of internal structure and local stresses on fracture propagation, deflection, and arrest in fault zones. J Struc Geol 32:1643–1655

Halder M, Paul D, Sensarma S (2021) Rhyolites in continental mafic large igneous provinces: petrology, geochemistry and petrogenesis. Geosci Front 12:53–80

Heiken G (1974) Atlas of volcanic ash. Smithsonian Contrib Earth Sci. https://doi.org/10.5479/si.00810274.12.1

Henry CD, Wolff JA (1992) Distinguishing strongly rheomorphic tuffs from extensive silicic lavas. Bull Volcanol 54:171–186

Kale VS, Bodas M, Chatterjee P, Pande K (2020) Emplacement history and evolution of the Deccan volcanic province, India. Episodes 43:278–299

Knott TR, Reichow MK, Branney MJ, Finn DR, Coe RS, Storey M, Bonnichsen B (2016) Rheomorphic ignimbrites of the Rogerson formation, central Snake River plain, USA: record of mid-Miocene rhyolitic explosive eruptions and associated crustal subsidence along the Yellowstone hotspot track. Bull Volcanol 78:23. https://doi.org/10.1007/s00445-016-1003-x

Korn H, Martin H (1954) The messum igneous complex in south west Africa. Trans Geol Soc S Afr 57:83–124

Krishnamacharlu T (1974) Ignimbrite flows from Rajula, Saurashtra, India. Geol Mag 111:49–54

Krishnamurthy P (2020) The Deccan volcanic province (DVP), India: a review. J Geol Soc Ind 96:9–35

Lele VS (1973) The Miliolite limestone of Saurashtra, western India. Sed Geol 10:301–310

Lenhardt N, Masango SM, Jolayemi OO, Lenhardt SZ, Peeters G-J, Eriksson PG (2017) The Palaeoproterozoic (~2.06 Ga) Rooiberg Group, South Africa: dominated by extremely high-grade lava-like and rheomorphic ignimbrites? New observations and lithofacies analysis. J Afr Earth Sci 131:213–232

Liesegang RE (1907) Über die bei Diffusionen auftretenden Schichtungen (the formation of layers during diffusion). Zeit Physikal Chem 59:444

Lipman PW (1976) Caldera-collapse breccias in the western San Juan Mountains, Colorado. Geol Soc Am Bull 87:1397–1410

Lipman PW (2000) Calderas. In: Sigurdsson H (ed) Encyclopedia of volcanoes. Academic Press, San Francisco, pp 643–662

Maithani PB, Banerjee R, Goyal N, Ramachandran S, Singh R (1995) Yttrium-, niobium- and zirconium-rich rhyolite dykes of Dhorio Nes area, district Jamnagar, Gujarat, India. Current Sci 69:270–272

Milner SC, Duncan AR, Ewart A (1992) Quartz latite rheoignimbrite flows of the Etendeka formation, north-western Namibia. Bull Volcanol 54:200–219

Misra KS (1999) Deccan volcanics in Saurashtra and Kutch, Gujarat, India. In: Subbarao KV (eds) Deccan volcanic province. Geol Soc Ind Mem 43. Geological Society of India, Bangalore, pp 325–334

Moore I, Kokelaar P (1998) Tectonically controlled piecemeal caldera collapse: a case study of Glencoe volcano, Scotland. Geol Soc Am Bull 110:1448–1466

Naik A, Sheth H, Sheikh JM, Kumar A (2021) Extremely high-grade, lava-like rhyolitic ignimbrites at Osham Hill, Saurashtra, northwestern Deccan Traps: stratigraphy, structures, textures, and physical volcanology. J Volcanol Geotherm Res 419:107389. https://doi.org/10.1016/j.jvolgeores.2021.107389

Ramsay JG (1967) Folding and fracturing of rocks. McGraw-Hill, New York, p 568

Ross CS, Smith RL (1961) Ash-flow tuffs: their origin, geologic relations and identification. US Geol Surv Prof Pap 366:81

Schmitt AK, Emmermann R, Trumbull RB, Bühn B, Henjes-Kunst F (2000) Petrogenesis and ^{40}Ar/^{39}Ar geochronology of the Brandberg Complex, Namibia: evidence for a major mantle contribution in metaluminous and peralkaline granites. J Petrol 41:1207–1239

Self S (2006) The effects and consequences of very large explosive volcanic eruptions. Phil Trans Roy Soc Lond (math Phys Eng Sci) 364:2073–2097

Sheikh JM, Sheth H, Naik A, Keluskar T (2020a) Widespread rheomorphic and lava-like silicic ignimbrites overlying flood basalts in the northwestern and northern Deccan Traps. Bull Volcanol 82:41. https://doi.org/10.1007/s00445-020-01381-9

Sheikh JM, Sheth H, Naik A, Keluskar T (2020b) Physical volcanology of the Pavagadh rhyolites, northern Deccan Traps: stratigraphic, structural, and textural record of explosive and effusive eruptions. J Volcanol Geotherm Res 404:107024. https://doi.org/10.1016/j.jvolgeores.2020.107024

Sheth H (2018) A photographic atlas of flood basalt volcanism. Springer, New York, p 363

Shrivastava PK (1968) Petrography and origin of Miliolite limestone of western Saurashtra coast. J Geol Soc Ind 9:88–96

Subba Rao S (1971) Petrogenesis of acid rocks of the Deccan Traps. Bull Volcanol 35:983–997

Verma SP, Torres-Alvarado IS, Sotelo-Rodriguez ZT (2002) SINCLAS: Standard igneous norm and volcanic rock classification system. Comput Geosci 28:711–715

Weber G, Castro JM (2017) Phase petrology reveals shallow magma storage prior to large explosive silicic eruptions at Hekla volcano, Iceland. Earth Planet Sci Lett 466:168–180

Williams H, McBirney AR (1979) Volcanology. Freeman, Cooper & Co., Berkeley, p 397

Wright JB (1985) The younger granites. In: Wright JB (ed) Geology and mineral resources of west Africa. Springer, pp 129–137